CHAPTER 75

Electric Properties of Nanostructures

K. Palotás, B. Lazarovits, P. Weinberger

*Center for Computational Materials Science,
Technical University of Vienna, Vienna, Austria*

L. Szunyogh

*Center for Computational Materials Science, Technical University of Vienna,
Vienna, Austria; and Department of Theoretical Physics, Center for Applied
Mathematics and Computational Physics Budapest University of Technology
and Economics, Budapest, Hungary*

CONTENTS

1. INTRODUCTION

This contribution is devoted to the theoretical description of the electric properties of nanostructured matter, in particular to structures nanoscaled in two dimensions, namely supported clusters of atoms such as finite chains of atoms embedded in the surface of a metallic substrate or atomic-sized contacts. Because this description is based on a "real space" representation of the so-called Kubo-Greenwood equation, it was felt necessary to give first a proper account of the theoretical background of linear response theory in terms of electric fields. For this reason Section 2 deals quite generally with currently available transport theories. In putting the Kubo-Greenwood equation into a computationally accessible scheme the use of density functional theory and multiple scattering approaches is required. Therefore only after having summarized very shortly the main quantities in a Korringa-Kohn-Rostoker-type realization of multiple scattering (Section 3), practical expressions for evaluating electric properties of nanostructures are introduced (Section 4). Clearly enough the numerical accuracy of such approaches have to be documented before any kind of application to nanosized matter can be given. Unfortunately this kind of numerical "test" leads back to bulk materials, for which the electric properties are well documented, both experimentally and theoretically. However, only the "tests" discussed in Section 5 provide the necessary confidence for the theoretical results presented in Sections 6 and 7 for finite wires and atomic-sized contacts.

   Not dealt with in this contributions are systems nanosized only in one dimension such as spin valves or other heterojunctions, as a review of such systems—also based on a Green's function realization of the Kubo-Greenwood equation—only appeared rather recently [1] that discusses in quite some length, for example, properties of the giant magnetoresistance (GMR).

2. TRANSPORT THEORIES

In this section, methods describing electric transport in solid matter are reviewed, with emphasis, however, on the Kubo-Greenwood approach. Consider a system of N interacting electrons moving in the electrostatic potential of the nuclei, the effective one-electron (Kohn-Sham-) Hamilton operator is then given by

$$\widehat{H}_0 = -\frac{\hbar^2}{2m} \sum_{i=1}^{N} \mathbf{\nabla}_i^2 + \sum_{i=1}^{N} u_{\text{eff}}(\mathbf{r}; \sigma, \mathcal{M}) \tag{1}$$

where the first term is the kinetic energy operator and the second the effective one-electron potential that in turn depends on the "spin" of the electrons (σ) as well as on the magnetic configuration of the system ($\mathcal{M}$). As it is well-known the corresponding one-electron Kohn-Sham equation can be written, e.g., in the case of a three-dimensional periodic system as

$$\widehat{H}_0 \phi_{k,\sigma}(\mathbf{r}) = E_{k,\sigma} \phi_{k,\sigma}(\mathbf{r}), \quad k = (\nu, \mathbf{k}) \tag{2}$$

where ν refers the so-called band index, $\mathbf{k}$ to the momentum, and $E_{k,\sigma}$ and $\phi_{k,\sigma}(\mathbf{r})$ denote the one-electron energies and states, respectively.

2.1. Boltzmann Formalism

This kind of theoretical approach assumes the existence of a distribution function $f_{k,\sigma}(\mathbf{r})$ that measures the probability of charge carriers with spin σ in state k in the neighborhood of $\mathbf{r}$. The change of $f_k(\mathbf{r})$,

$$f_k(\mathbf{r}) = \sum_\sigma f_{k,\sigma}(\mathbf{r})$$

in time is then described by the famous *Boltzmann equation*,

$$\left(\frac{\partial f_k(\mathbf{r},t)}{\partial t}\right) + \left(\frac{\partial f_k(\mathbf{r})}{\partial t}\right)_{\text{diffusion}} + \left(\frac{\partial f_k(\mathbf{r})}{\partial t}\right)_{\text{field}} = -\left(\frac{\partial f_k(\mathbf{r})}{\partial t}\right)_{\text{scattering}} \tag{3}$$

in which the various terms correspond to different effects, namely from the left to right: an explicit time dependence, diffusion, the influence of external fields and scattering. Stationarity implies now that the total time dependence of $f_k(\mathbf{r})$ vanishes, see Eq. (3).

For matters of simplicity in the following the $\mathbf{r}$-dependence of the distribution function will be neglected. The local change of electrons resulting from elastic scattering of independent particles can be correlated to the *microscopic scattering probability*,

$$P_{k\sigma,k'\sigma'} = \begin{pmatrix} P_{k\uparrow,k'\uparrow} & P_{k\uparrow,k'\downarrow} \\ P_{k\downarrow,k'\uparrow} & P_{k\downarrow,k'\downarrow} \end{pmatrix} \tag{4}$$

in the following manner

$$\left(\frac{\partial f_k}{\partial t}\right)_{\text{scattering}} = \sum_\sigma \sum_{k'\sigma'}[f_{k',\sigma'}(1-f_{k,\sigma})P_{k'\sigma',k\sigma} - (1-f_{k',\sigma'})f_{k,\sigma}P_{k\sigma,k'\sigma'}] \tag{5}$$

The first contribution is usually called *scattering-in term* and describes the scattering of electrons from occupied states (k',σ') into an empty state (k,σ); the second term refers to the reverse process, namely the scattering of an electron from an occupied state (k,σ) into empty states (k',σ') and is called *scattering-out term*. It therefore seems reasonable to separate the distribution function into two parts,

$$f_{k,\sigma} = f^0_{k,\sigma} + g_{k,\sigma} \tag{6}$$

where

$$f^0_{k,\sigma} = \frac{1}{e^{\beta(E_{k,\sigma}-E_F)}+1} \tag{7}$$

is the Fermi-Dirac distribution function with $E_{k,\sigma}$ denoting the one-electron energies, see Eq. (2), E_F the Fermi energy, and $\beta = 1/k_B T$ with k_B being the Boltzmann constant and T the temperature. In Eq. (6) $g_{k,\sigma}$ denotes the deviation from the equilibrium distribution function. Making use of the *principle of microscopic reversibility*,

$$P_{k\sigma,k'\sigma'} = P_{k'\sigma',k\sigma}$$

for the microscopic scattering probabilities and the separation of $f_{k,\sigma}$ in Eq. (6), the scattering term in Eq. (5) can be rewritten as

$$\left(\frac{\partial f_k}{\partial t}\right)_{\text{scattering}} = \sum_\sigma \sum_{k'\sigma'} P_{k\sigma,k'\sigma'}(g_{k',\sigma'} - g_{k,\sigma}) \tag{8}$$

Neglecting now in Eq. (3) terms with an explicit time dependence of the distribution function and changes caused by diffusion, that is, keeping only changes of f_k arising from a homogeneous external electric field $\mathbf{E}$, the following expression is obtained,

$$e\sum_\sigma \left(\frac{\partial f^0_{k,\sigma}}{\partial E_{k,\sigma}}\right)\mathbf{v}_{k,\sigma}\mathbf{E} = \sum_\sigma \sum_{k'\sigma'} P_{k\sigma,k'\sigma'}(g_{k',\sigma'} - g_{k,\sigma}) \tag{9}$$

where $\mathbf{v}_{k,\sigma}$ is the velocity of the electrons with spin σ, which in turn can be related semi-classically to the one-electron energies as follows

$$\mathbf{v}_{k,\sigma} = \frac{1}{\hbar}\frac{\partial E_{k,\sigma}}{\partial \mathbf{k}} \tag{10}$$

Assuming that $g_{k,\sigma}$ depends linearly on the external electric field, the following *ansatz* can be made,

$$g_{k,\sigma} = -e\left(\frac{\partial f^0_{k,\sigma}}{\partial E_{k,\sigma}}\right)\Lambda_{k,\sigma}\mathbf{E} \tag{11}$$

where $\Lambda_{k,\sigma}$ is the so-called *mean free path vector* of electrons of spin σ. The magnitude of $\Lambda_{k,\sigma}$ measures the path of an electron with spin σ between two scattering events.

By introducing a so-called *relaxation time* $\tau_{k,\sigma}$, which specifies the time that an electron stays in state (k,σ) until the next scattering event (*scattering life time*) occurs as

$$\tau^{-1}_{k,\sigma} = \sum_{k'\sigma'} P_{k\sigma,k'\sigma'} \tag{12}$$

Eq. (9) can be solved with the ansatz in Eq. (11) to give

$$\Lambda_{k,\sigma} = \tau_{k,\sigma}\left(\mathbf{v}_{k,\sigma} + \sum_{k'\sigma'} P_{k\sigma,k'\sigma'}\Lambda_{k',\sigma'}\right) \tag{13}$$

This now is a system of coupled integral equations. The different spin-components can be decoupled by ignoring *spin-flip scattering processes*, namely assuming in Eq. (4) that

$$P_{k\uparrow,k'\downarrow} = 0, \quad P_{k\downarrow,k'\uparrow} = 0$$

such that a relatively simple integral equation is obtained,

$$\Lambda_{k,\sigma} = \tau_{k,\sigma}\left(\mathbf{v}_{k,\sigma} + \sum_{k'} P_{k\sigma,k'\sigma}\Lambda_{k',\sigma}\right) \tag{14}$$

from which in principle $\Lambda_{k,\sigma}$ can be evaluated.

Due to the neglect of *spin-flip scattering processes*, the total current density can be written as

$$\mathbf{j} = \sum_{\sigma}\mathbf{j}_{\sigma} = \frac{e}{V}\sum_{k,\sigma} f_{k,\sigma}\mathbf{v}_{k,\sigma} \tag{15}$$

where V is the volume of the system. The *conductivity tensor* $\underline{\underline{\sigma}}$ at $T = 0$ is then obtained by using *Ohm's law*, $\mathbf{j}_{\sigma} = \underline{\underline{\sigma}}_{\sigma}\mathbf{E}$, and Eqs. (6), (11), (15),

$$\underline{\underline{\sigma}} = \sum_{\sigma}\underline{\underline{\sigma}}_{\sigma} = \frac{e^2}{V}\sum_{k,\sigma}\delta(E_{k,\sigma} - E_F)\mathbf{v}_{k,\sigma}\circ\Lambda_{k,\sigma} \tag{16}$$

where $\circ$ denotes a dyadic product (resulting in a 3×3 tensor). The contributions to the total conductivity refer therefore to independent *majority* ($\uparrow$) and *minority* ($\downarrow$) spin channels (*two current model* [2]).

Neglecting the scattering-in term in Eq. (13), the conductivity is finally given by

$$\underline{\underline{\sigma}} = \sum_{\sigma}\underline{\underline{\sigma}}_{\sigma} = \frac{e^2}{V}\sum_{k,\sigma}\delta(E_{k,\sigma} - E_F)\tau_{k,\sigma}\mathbf{v}_{k,\sigma}\circ\mathbf{v}_{k,\sigma} \tag{17}$$

where

$$\sum_{k,\sigma}\delta(E_{k,\sigma} - E_F) = n(E_F) \tag{18}$$

is nothing but the density of states at the Fermi energy. Obviously the conductivity tensor is determined by three factors: the density of states, the velocities, and the relaxation times of the electrons at the Fermi surface. While the first two factors arise from the electronic structure of the system, the last one refers to defects or impurities present in the solid. Moreover, different approximations can be made for the relaxation time in Eq. (17), for example, an isotropic τ, or spin-dependent τ_σ, thus resulting in a simple expression for the conductance.

It has to be mentioned that the Boltzmann equation can easily be implemented within traditional bulk bandstructure methods, since in the semi-classical interpretation the velocity is given by the energy dispersion, see Eq. (10). Apart from being a semi-classical theory, the main disadvantages is that in the form of Eq. (17) only ordered bulk systems (three-dimensional cyclic boundary conditions) can be described, as a welldefined Fermi surface is needed and the relaxation times are system-dependent parameters.

2.2. Landauer Formalism

The *Landauer-Büttiker approach* [3, 4] is an effective tool to describe transport in mesoscopic systems. Suppose a multiprobe structure consists of a finite region connected to N_L leads, each lead being attached to an ideal "reservoir." The electrons are then scattered in a finite region (*scattering or interaction region*) caused either by disorder or due to a particular geometry. The transport through the scattering region is thought to be completely coherent, no phase breaking is taken into account, and because of assumed low temperatures inelastic scattering processes are supposed to be negligible. The leads are used to inject and drain current or measure voltage, whereas the reservoirs are assumed to fulfil certain conditions: the reservoir for the nth lead has to be in equilibrium at a given chemical potential μ_n,

$$\mu_n = E_F + eV_n \tag{19}$$

where V_n is the applied potential and E_F the Fermi energy. Furthermore, a steady-state current flowing from/into the reservoir is supposed not to change μ_n implying of course large enough reservoirs. Moreover, it is assumed that no additional resistance is produced by the interface between a reservoir and the scattering region. This in turn implies that an electron that enters a reservoir must be scattered inelastically before returning to the coherent scattering region, providing thus a phase-randomization. The current passsing through the nth lead can be written as

$$I_n = \sum_{m \neq n} g_{nm} V_m \tag{20}$$

where the sum extends over all leads except the nth one, and the g_{nm} are the so-called conductance coefficients of the system.

Introducing incoming and outgoing scattering channels which play the same role as incoming and outgoing Bloch states in scattering theory, the conductance can be expressed in terms of a transmission probability ($T_{ni, mj}$) or S-matrix ($S_{ni, mj}$) as

$$g_{nm} = \frac{2e^2}{h} \sum_{ij} T_{ni, mj} = \frac{2e^2}{h} \sum_{ij} |S_{ni, mj}|^2 \tag{21}$$

In this equation $T_{ni, mj}$ is the transmission probability for an electron from an incoming channel j in lead m to an outgoing channel i in lead n, the factor 2 accounts for the two spin directions, and the sum has to be carried out over all incoming and outgoing channels in the corresponding leads.

The advantage of using the Landauer formalism is first and foremost seen for two-probe structures, for which only one conductance coefficient g has to be considered such as, for example, in the case of perpendicular transport (current perpendicular to plane-CPP) in layered structures or for quantum point-contacts. The main parameters of a contact refer to the characteristic lengths of the system, namely the *contact diameter* (d) and the *mean free path for elastic* (Λ_e) and *inelastic* (Λ_i) scattering, that is, the length of an electron's

path between two elastic (inelastic) scattering events. If $d \ll \Lambda_e$, Λ_i one speaks of a *ballistic point-contact*, as an electron travels through the contact without any scattering. If $d \gg \Lambda_e$ a point-contact is said to belong to the *diffusive* regime meaning that an electron experiences a lot of elastic scattering when traveling through the contact. In both cases the contact diameter must be much larger than the electron's wavelength.

In the case of *two-probe structures* the conductance can be written according to Eq. (21) as

$$g = \frac{2e^2}{h} \sum_{ij} T_{ij} \tag{22}$$

where T_{ij} is a hermitian matrix. Diagonalized the conductance can be formulated in the eigenchannel basis as

$$g = \frac{2e^2}{h} \sum_{i=1}^{N} T_i \tag{23}$$

where N is the number of conducting channels and the T_i are the real eigenvalues of T_{ij}, $0 < T_i < 1$. For an *ideal ballistic point-contact* as well as for the theoretically interesting case of an infinite periodic wire, $T_{ij} = \delta_{ij}$ which implies that the conductance is quantized in units of the so-called conductance quantum $G_0 = 2e^2/h$,

$$g = N_{ch} G_0 \tag{24}$$

Such quantized conductances have been observed by many experimental groups. Within the Landauer approach, the conductance obviously depends on the *number of open eigenchannels* N_{ch}, which in turn depends on the sample geometry. This implies that N_{ch} is determined for the entire system by the *narrowest cross section* of a point-contact or a wire.

2.3. Kubo Formalism

In the 1950s, Kubo developed a method of evaluating the response of a quantum mechanical system to an external potential, in particular, the current in response to an electric field [5]. To first order, known as linear response, the two quantities are related by a conductivity (Ohm's law), which is given in terms of the equilibrium properties of the system, that is, in the limit of a vanishing field. Moreover, conductance coefficients can be derived from the conductivity, which describes the total current flowing in and out of the system in response to the voltages applied.

2.3.1. Linear Response Theory

2.3.1.1. Linear Response and the Green Function   Assuming a time-dependent perturbation $\widehat{H}'(t)$, the Hamilton operator of the perturbed system is of the form,

$$\widehat{H}(t) = \widehat{H}_0 + \widehat{H}'(t) \tag{25}$$

For a grand-canonical ensemble the density operator of the unperturbed system can be written as

$$\hat{\varrho}_0 = \frac{1}{\mathcal{Z}} e^{-\beta \widehat{\mathcal{H}}_0} \tag{26}$$

with

$$\widehat{\mathcal{H}}_0 = \widehat{H}_0 - \mu \widehat{N} \tag{27}$$

where μ is the chemical potential, $\widehat{N}$ the (particle) number operator, and $\mathcal{Z}$ is the grand canonical partition function,

$$\mathcal{Z} = Tr(e^{-\beta \widehat{\mathcal{H}}_0}) \tag{28}$$

Because the expectation value of a physical observable A, associated with a hermitian operator $\widehat{A}$ corresponding to the unperturbed system is given by

$$A_0 = \langle A \rangle = \frac{1}{\mathcal{Z}} Tr(\widehat{A} e^{-\beta \widehat{\mathcal{H}}_0}) = Tr(\hat{\varrho}_0 \widehat{A}) \tag{29}$$

within the Schrödinger picture the equation of motion for the density operator can be written as

$$i\hbar \frac{\partial \hat{\varrho}(t)}{\partial t} = [\widehat{\mathscr{H}}(t), \hat{\varrho}(t)] \tag{30}$$

where

$$\widehat{\mathscr{H}}(t) = \widehat{H}(t) - \mu \widehat{N} = \widehat{\mathscr{H}}_0 + \widehat{H}'(t) \tag{31}$$

Clearly enough, in the absence of a perturbation, $\hat{\varrho}(t) = \hat{\varrho}_0$. Therefore, partitioning $\hat{\varrho}(t)$ as

$$\hat{\varrho}(t) = \hat{\varrho}_0 + \hat{\varrho}'(t) \tag{32}$$

and making use of the fact that $[\widehat{\mathscr{H}}_0, \hat{\varrho}_0] = 0$, one gets in first order in $\widehat{H}'$,

$$i\hbar \frac{\partial \hat{\varrho}'(t)}{\partial t} = [\widehat{\mathscr{H}}_0, \hat{\varrho}'(t)] + [\widehat{H}'(t), \hat{\varrho}_0] \tag{33}$$

or, by switching to the interaction (Dirac) picture,

$$\hat{\varrho}_D(t) = \hat{\varrho}_0 + \hat{\varrho}'_D(t), \quad \hat{\varrho}'_D(t) = e^{(i/\hbar)\widehat{\mathscr{H}}_0 t} \hat{\varrho}'(t) e^{-(i/\hbar)\widehat{\mathscr{H}}_0 t} \tag{34}$$

$$i\hbar \frac{\partial \hat{\varrho}'_D(t)}{\partial t} = [\widehat{H}'_D(t), \hat{\varrho}_0] \tag{35}$$

This equation has to be solved now for a given initial condition. Turning on the external field adiabatically at $t = -\infty$, implies that the density operator of the system at $t = -\infty$ represents an ensemble of systems in thermal equilibrium, that is,

$$\lim_{t \to -\infty} \hat{\varrho}(t) = \hat{\varrho}_0, \quad \lim_{t \to -\infty} \hat{\varrho}'_D(t) = 0$$

Using this boundary condition for $\hat{\varrho}'_D(t)$ results into the following integral equation

$$\hat{\varrho}'_D(t) = -\frac{i}{\hbar} \int_{-\infty}^{t} dt' [\widehat{H}'_D(t'), \hat{\varrho}_0] \tag{36}$$

such that in the Schrödinger picture the density operator can be approximated in first order as

$$\hat{\varrho}(t) \approx \hat{\varrho}_0 - \frac{i}{\hbar} \int_{-\infty}^{t} dt' e^{-(i/\hbar)\widehat{\mathscr{H}}_0 t} [\widehat{H}'_D(t'), \hat{\varrho}_0] e^{(i/\hbar)\widehat{\mathscr{H}}_0 t} \tag{37}$$

Considering now the time evolution of the physical observable $A(t)$,

$$A(t) = Tr(\hat{\varrho}(t)\widehat{A}) = A_0 - \frac{i}{\hbar} \int_{-\infty}^{t} dt' \, Tr\big(e^{-(i/\hbar)\widehat{\mathscr{H}}_0 t}[\widehat{H}'_D(t'), \hat{\varrho}_0] e^{(i/\hbar)\widehat{\mathscr{H}}_0 t} \widehat{A}\big)$$

$$= A_0 - \frac{i}{\hbar} \int_{-\infty}^{t} dt' \, Tr\big([\widehat{H}'_D(t'), \hat{\varrho}_0] \widehat{A}_D(t)\big) \tag{38}$$

where A_0 is defined in Eq. (29) and the Dirac representation of operator $\widehat{A}$ is given by

$$\widehat{A}_D(t) = e^{(i/\hbar)\widehat{\mathscr{H}}_0 t} \widehat{A} e^{-(i/\hbar)\widehat{\mathscr{H}}_0 t} \tag{39}$$

then by making use of the identity,

$$Tr([\widehat{A}, \widehat{B}]\widehat{C}) = Tr(\widehat{A}\widehat{B}\widehat{C} - \widehat{B}\widehat{A}\widehat{C}) = Tr(\widehat{B}\widehat{C}\widehat{A} - \widehat{B}\widehat{A}\widehat{C}) = Tr(\widehat{B}[\widehat{C}, \widehat{A}])$$

one arrives at

$$\delta A(t) = A(t) - A_0 = -\frac{i}{\hbar} \int_{-\infty}^{t} dt' \, Tr\big(\hat{\varrho}_0 [\widehat{A}_D(t), \widehat{H}'_D(t')]\big) \tag{40}$$

Assuming finally that the perturbation $\widehat{H}'(t)$ is of the form,

$$\widehat{H}'(t) = \widehat{B}F(t) \tag{41}$$

where $\widehat{B}$ is a *Hermitian operator* and $F(t)$ is a *complex function* (classical field), Eq. (40) transforms to

$$\delta A(t) = -\frac{i}{\hbar}\int_{-\infty}^{t}dt'\, F(t')Tr\big(\hat{\varrho}_0\big[\widehat{A}_D(t),\widehat{B}_D(t')\big]\big) \tag{42}$$

which can be written in terms of a *retarded Green function as*,

$$G_{AB}^{\text{ret}}(t,t') = -i\Theta(t-t')Tr\big(\hat{\varrho}_0\big[\widehat{A}_D(t),\widehat{B}_D(t')\big]\big) \tag{43}$$

or, by introducing a so-called generalized susceptibility,

$$\chi_{AB}(t,t') = \frac{1}{\hbar}G_{AB}^{\text{ret}}(t,t') \tag{44}$$

as

$$\delta A(t) = \frac{1}{\hbar}\int_{-\infty}^{\infty}dt'\, F(t')G_{AB}^{\text{sret}}(t,t') = \int_{-\infty}^{\infty}dt'\, F(t')\chi_{AB}(t,t') \tag{45}$$

Suppose now that the operators $\widehat{A}$ and $\widehat{B}$ do not depend explicitly on time, then $G_{AB}^{\text{ret}}(t,t')$ and $\chi_{AB}(t,t')$ are only functions of the argument $(t-t')$. Consequently, the Fourier coefficients of $\delta A(t)$ can be written as

$$\delta A(\omega) = \frac{1}{\hbar}F(\omega)G_{AB}^{\text{ret}}(\omega) = F(\omega)\chi_{AB}(\omega) \tag{46}$$

where

$$X(\omega) = \int_{-\infty}^{\infty}dt\, X(t)e^{i\omega t}, \quad X(t) = \frac{1}{2\pi}\int_{-\infty}^{\infty}d\omega\, X(\omega)e^{-i\omega t} \tag{47}$$

applies for any time-dependent quantity $X(t)$.

Because by definition $G_{AB}^{\text{ret}}(\omega)$ is analytical only in the upper complex semi-plane (retarded sheet), for a real argument ω the limit $\varpi \to \omega + i0$ has to be considered. The *complex admittance* $\chi_{AB}(\omega)$ can therefore be expressed in terms of the retarded Green function as

$$\chi_{AB}(\omega) = \frac{1}{\hbar}G_{AB}^{\text{ret}}(\omega+i0) = -\frac{i}{\hbar}\int_{0}^{\infty}dt\, e^{i(\omega+i0)t}Tr\big(\hat{\varrho}_0\big[\widehat{A}(t),\widehat{B}(0)\big]\big) \tag{48}$$

The occurance of the side-limit $\omega + i0$ in $\chi_{AB}(\omega)$ is usually termed adiabatic switching on of the perturbation as it corresponds to a time-dependent classical field,

$$F'(t) = \lim_{s\to+0}\big(F(t)e^{st}\big) \tag{49}$$

2.3.1.2. The Kubo Formula   Returning now to Eq. (38),

$$\delta A(t) = -\frac{i}{\hbar}\int_{-\infty}^{t}dt'\, Tr\big(\big[\widehat{H}'_H(t'),\hat{\varrho}_0\big]\widehat{A}_H(t)\big) \tag{50}$$

where the operators are defined within the Heisenberg picture with respect to the unperturbed system and using *Kubo's identity*,

$$\frac{i}{\hbar}[\widehat{X}_H(t),\hat{\varrho}] = \hat{\varrho}\int_{0}^{\beta}d\lambda\,\dot{\widehat{X}}_H(t-i\lambda\hbar),$$

$$\hat{\varrho} = \frac{e^{-\beta\widehat{H}}}{Tr\big(e^{-\beta\widehat{H}}\big)}, \quad \widehat{X}_H(t) = e^{(i/\hbar)\widehat{H}t}\widehat{X}(t)e^{-(i/\hbar)\widehat{H}t}, \quad \dot{\widehat{X}}_H(t) = -\frac{i}{\hbar}[\widehat{X}_H(t),\widehat{H}] \tag{51}$$

in Eq. (50) finally yields the famous *Kubo formula*:

$$\delta A(t) = -\int_{-\infty}^{t} dt' \int_{0}^{\beta} d\lambda \, Tr\big(\hat{\varrho}_0 \dot{\widehat{H}}'_H(t'-i\lambda\hbar)\widehat{A}_H(t)\big)$$

$$= -\int_{-\infty}^{t} dt' \int_{0}^{\beta} d\lambda \, Tr\big(\hat{\varrho}_0 \dot{\widehat{H}}'(t')\widehat{A}_H(t-t'+i\lambda\hbar)\big) \tag{52}$$

2.3.2. The Current-Current Correlation Function

In the case of electric transport, a time-dependent external electric field is applied. Obviously, this induces currents, which in turn creates internal electric fields. Suppose that the total electric field, $\mathbf{E}(\mathbf{r}, t)$ is related to the perturbation, $\widehat{H}'(t)$ in terms of a scalar potential $\phi(\mathbf{r}, t)$ as

$$\widehat{H}'(t) = \int d^3r \, \hat{\rho}(\mathbf{r})\phi(\mathbf{r}, t), \quad \mathbf{E}(\mathbf{r}, t) = -\boldsymbol{\nabla}\phi(\mathbf{r}, t) \tag{53}$$

where $\hat{\rho}(\mathbf{r}) = e\psi(\mathbf{r})^{+}\psi(\mathbf{r})$ is the charge density operator, $\psi(\mathbf{r})$ a field operator and e the charge of an electron. Then the time-derivative of $\widehat{H}'_H(t)$ can be calculated as follows,

$$\dot{\widehat{H}}'(t) = \int d^3r \, \underbrace{\frac{1}{i\hbar}\big[\widehat{\mathscr{H}}_0, \hat{\rho}(\mathbf{r})\big]}_{\frac{\partial \hat{\rho}_H(\mathbf{r},t)}{\partial t}|_{t=0}} \phi(\mathbf{r}, t) = -\int d^3r \, \boldsymbol{\nabla}\widehat{\mathbf{J}}(\mathbf{r})\,\phi(\mathbf{r}, t)$$

$$= \int d^3r \, \widehat{\mathbf{J}}(\mathbf{r})\,\boldsymbol{\nabla}\phi(\mathbf{r}, t) = -\int d^3r \, \widehat{\mathbf{J}}(\mathbf{r})\,\mathbf{E}(\mathbf{r}, t) \tag{54}$$

where the current-density operator is given by

$$\widehat{\mathbf{J}}(\mathbf{r}) = \begin{cases} \dfrac{e\hbar}{2mi}\psi(\mathbf{r})^{+}(\overrightarrow{\nabla} - \overleftarrow{\nabla})\psi(\mathbf{r}), & \text{in non-relativistic case,} \\[2mm] ec\psi(\mathbf{r})^{+}\,\hat{\boldsymbol{\alpha}}\,\psi(\mathbf{r}), & \text{in relativistic case} \end{cases} \tag{55}$$

and the $\hat{\boldsymbol{\alpha}}$ denote Dirac matrices. Note that in Eq. (54) the continuity equation was used and periodic boundary conditions were assumed such that when using Gauss' integration theorem the corresponding surface term vanishes. Making use of Eqs. (52) and (54), the μth component of the current density can be written as

$$J_\mu(\mathbf{r}, t) = \sum_\nu \int d^3r' \int_{-\infty}^{\infty} dt' \sigma_{\mu\nu}(\mathbf{r}, \mathbf{r}'; t, t')\, E_\nu(\mathbf{r}', t') \tag{56}$$

where the occurring space-time correlation function is given by

$$\sigma_{\mu\nu}(\mathbf{r}, \mathbf{r}'; t, t') = \Theta(t - t')\int_{0}^{\beta} d\lambda \, Tr\big(\hat{\varrho}_0 \widehat{J}_\nu(\mathbf{r}, 0)\widehat{J}_\mu(\mathbf{r}', t-t'+i\lambda\hbar)\big) \tag{57}$$

by which the linear response of the current density at $(\mathbf{r}, t)$ in direction μ is correlated to the local electric field at $(\mathbf{r}', t')$ applied in direction ν. Note that in the above equation the current-density operators are assumed to be Heisenberg operators.

Consider now the Fourier components of the electric field,

$$\mathbf{E}(\mathbf{q}, \omega) = \int d^3r \int_{-\infty}^{\infty} dt \, \mathbf{E}(\mathbf{r}, t)e^{-i\mathbf{q}\cdot\mathbf{r}+i\varpi t} \tag{58}$$

$$\mathbf{E}(\mathbf{r}, t) = \frac{1}{2\pi V}\int d^3q \int_{-\infty}^{\infty} d\omega \, \mathbf{E}(\mathbf{q}, \omega)e^{i\mathbf{q}\cdot\mathbf{r}-i\varpi t} \tag{59}$$

where $\varpi = \omega + i0$ and V is the volume of the system. Although $\sigma_{\mu\nu}(\mathbf{r}, \mathbf{r}'; t, t')$ trivially depends only on $(t - t')$, in general, it is a function of the independent space variables $\mathbf{r}$ and $\mathbf{r}'$. In cases, however, the current density is an average of the local current density in Eq. (56) over a large enough region, $\sigma_{\mu\nu}(\mathbf{r}, \mathbf{r}'; t, t')$ can be assumed to be homogeneous in space, that is, $\sigma_{\mu\nu}(\mathbf{r}, \mathbf{r}'; t - t') = \sigma_{\mu\nu}(\mathbf{r} - \mathbf{r}'; t - t')$. This usually is the case if $|\mathbf{q}|$ is small,

implying that *long-wavelength excitations* are studied. The $(\mathbf{q}, \omega)$ component of the current density per unit volume,

$$J_\mu(\mathbf{q}, \omega) = \frac{1}{V} \int d^3 r \int_{-\infty}^{\infty} dt \, J_\mu(\mathbf{r}, t) e^{-i\mathbf{q} \cdot \mathbf{r} + i\varpi t} \tag{60}$$

can then be determined from Eqs. (56) and (57),

$$J_\mu(\mathbf{q}, \omega) = \sum_\nu \sigma_{\mu\nu}(\mathbf{q}, \omega) \, E_\nu(\mathbf{q}, \omega) \tag{61}$$

where $\sigma_{\mu\nu}(\mathbf{q}, \omega)$ is the *wave-vector* and *frequency-dependent conductivity tensor*,

$$\sigma_{\mu\nu}(\mathbf{q}, \omega) = \frac{1}{V} \int_0^{\infty} dt \, e^{i\varpi t} \int_0^{\beta} d\lambda \, Tr\big(\hat{\varrho}_0 \widehat{J}_\nu(-\mathbf{q}, 0) \widehat{J}_\mu(\mathbf{q}, t + i\lambda\hbar)\big) \tag{62}$$

and

$$J_\mu(\mathbf{q}, t) = \int d^3 r \, J_\mu(\mathbf{r}, t) e^{-i\mathbf{q} \cdot \mathbf{r}} \tag{63}$$

In using contour integration techniques one arrives at

$$\sigma_{\mu\nu}(\mathbf{q}, \omega) = \frac{i}{\hbar V} \int_0^{\infty} dt \, e^{i\varpi t} \int_t^{\infty} dt' \, Tr\big(\hat{\varrho}_0 [\widehat{J}_\mu(\mathbf{q}, t'), \widehat{J}_\nu(-\mathbf{q}, 0)]\big) \tag{64}$$

such that by introducing the below *current-current correlation function*,

$$\Sigma_{\mu\nu}(\mathbf{q}, \varpi) = \frac{1}{\hbar V} \int_0^{\infty} dt \, e^{i\varpi t} \, Tr\big(\hat{\varrho}_0 [\widehat{J}_\mu(\mathbf{q}, t), \widehat{J}_\nu(-\mathbf{q}, 0)]\big) \tag{65}$$

the conductivity tensor can finally be expressed as

$$\sigma_{\mu\nu}(\mathbf{q}, \omega) = \frac{\Sigma_{\mu\nu}(\mathbf{q}, \varpi) - \Sigma_{\mu\nu}(\mathbf{q}, 0)}{\varpi} \tag{66}$$

For a homogeneous system with carrier density n and mass of carriers m,

$$-\frac{\Sigma_{\mu\nu}(\mathbf{q}, 0)}{\varpi} = i \frac{ne^2}{m\varpi} \delta_{\mu\nu} \tag{67}$$

one obtains the phenomenological Drude term for noninteracting particles. Furthermore, the *static limit*, that is, when $\omega \to 0$ and $|\mathbf{q}| \to 0$, is defined as

$$\begin{aligned} \sigma_{\mu\nu}(\mathbf{q} = 0, \omega = 0) &= \lim_{s \to +0} \frac{\Sigma_{\mu\nu}(\mathbf{q} = 0, is) - \Sigma_{\mu\nu}(\mathbf{q} = 0, 0)}{is} \\ &= \frac{d\,\Sigma_{\mu\nu}(\mathbf{q} = 0, \varpi)}{d\varpi}\bigg|_{\varpi = 0} \end{aligned} \tag{68}$$

2.3.3. Kubo Formula for Independent Particles

An important special case arises when considering independent particles. Represented in the basis of the eigenfuctions of $\widehat{H}_0$ (spectral representation),

$$\widehat{H}_0 |n\rangle = \varepsilon_n |n\rangle, \quad \langle m|n\rangle = \delta_{nm}, \quad \sum_n |n\rangle\langle n| = \widehat{I} \tag{69}$$

the equilibrium density operator and its matrix elements are given by

$$\hat{\varrho}_0 = \sum_n f(\varepsilon_n) |n\rangle\langle n|, \quad \langle n|\hat{\varrho}_0|p\rangle = f(\varepsilon_n) \delta_{pn} \tag{70}$$

and the thermal average of the current–current commutator can be written as

$$\begin{aligned} Tr\big(\hat{\varrho}_0 [\widehat{J}_\mu(\mathbf{q}, t'), \widehat{J}_\nu(-\mathbf{q}, 0)]\big) = \sum_{nm} \{f(\varepsilon_n) - f(\varepsilon_m)\} e^{(i/\hbar)(\varepsilon_n - \varepsilon_m)t'} \\ \times J_\mu^{nm}(\mathbf{q}) J_\nu^{mn}(-\mathbf{q}) \end{aligned} \tag{71}$$

with

$$J_\mu^{nm}(\mathbf{q}) \equiv \langle n|\widehat{J}_\mu(\mathbf{q})|m\rangle \quad \text{and} \quad J_\nu^{mn}(-\mathbf{q}) \equiv \langle m|\widehat{J}_\nu(-\mathbf{q})|n\rangle \qquad (72)$$

Substituting Eq. (71) into Eq. (65) then yields

$$\Sigma_{\mu\nu}(\mathbf{q}, \omega) = \frac{1}{\hbar V} \sum_{nm} \{f(\varepsilon_n) - f(\varepsilon_m)\} J_\mu^{nm}(\mathbf{q}) J_\nu^{mn}(-\mathbf{q}) \int_0^\infty dt\, e^{(i/\hbar)(\varepsilon_n - \varepsilon_m + \hbar\varpi)t} \qquad (73)$$

The integral with respect to t, however, is just the Laplace transform of the identity,

$$\int_0^\infty dt\, e^{[(i/\hbar)(\varepsilon_n - \varepsilon_m + \hbar\omega) - s]t} \underset{(s>0)}{=} -\frac{e^{[(i/\hbar)(\varepsilon_n - \varepsilon_m + \hbar\omega) - s]}}{(i/\hbar)(\varepsilon_n - \varepsilon_m + \hbar\omega) - s} \qquad (74)$$

therefore, Eq. (73) can be transformed to

$$\Sigma_{\mu\nu}(\mathbf{q}, \omega) = \frac{i}{V} \sum_{nm} \frac{f(\varepsilon_n) - f(\varepsilon_m)}{\varepsilon_n - \varepsilon_m + \hbar\varpi} J_\mu^{nm}(\mathbf{q}) J_\nu^{mn}(-\mathbf{q}) \qquad (75)$$

with $f(\varepsilon)$ being the Fermi-Dirac function. Together with Eq. (64), this now provides a numerically tractable tool to calculate the conductivity tensor. Because

$$\frac{1}{\varepsilon_n - \varepsilon_m + \hbar\varpi} - \frac{1}{\varepsilon_n - \varepsilon_m} = \frac{-\hbar\varpi}{(\varepsilon_n - \varepsilon_m)(\varepsilon_n - \varepsilon_m + \hbar\varpi)}$$

$\sigma_{\mu\nu}(\mathbf{q}, \omega)$ can also be written in the following compact form,

$$\sigma_{\mu\nu}(\mathbf{q}, \omega) = \frac{\hbar}{iV} \sum_{nm} \frac{f(\varepsilon_n) - f(\varepsilon_m)}{\varepsilon_n - \varepsilon_m} \frac{J_\mu^{nm}(\mathbf{q}) J_\nu^{mn}(-\mathbf{q})}{\varepsilon_n - \varepsilon_m + \hbar\varpi},$$

$$\varpi = \omega + i\delta \qquad (76)$$

2.3.4. Contour Integrations

$\Sigma_{\mu\nu}(\mathbf{q}, \varpi)$ can be evaluated by using contour integration techniques. Considering a pair of eigenvalues, ε_n and ε_m, for a suitable contour C in the complex energy plane (see Fig. 1) the residue theorem implies that

$$\oint_C dz \frac{f(z)}{(z - \varepsilon_n)(z - \varepsilon_m + \hbar\omega + i\delta)} = -2\pi i \frac{f(\varepsilon_n)}{\varepsilon_n - \varepsilon_m + \hbar\omega + i\delta}$$

$$+ 2i\delta_T \sum_{k=-N_2+1}^{N_1} \frac{1}{(z_k - \varepsilon_n)(z_k - \varepsilon_m + \hbar\omega + i\delta)} \qquad (77)$$
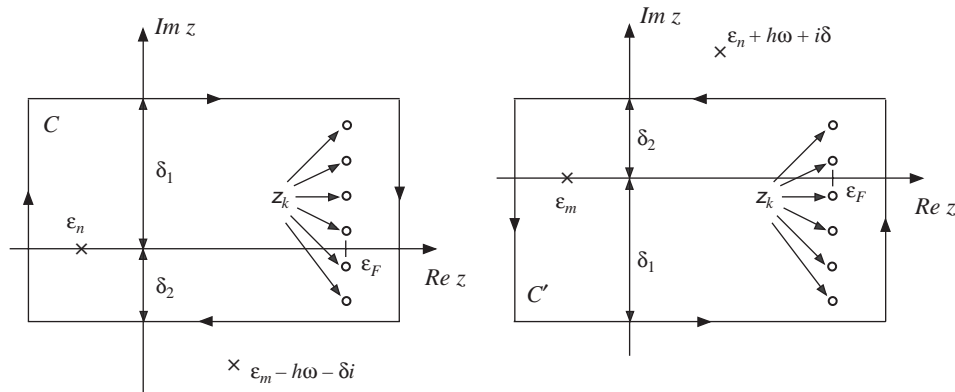

Figure 1. Integrations along the contours C (left entry) and C' (right entry).

where the $z_k = E_F + i(2k-1)\delta_T$ are the (fermionic) Matsubara-poles with E_F being the Fermi energy, $\delta_T \equiv \pi k_B T$ and T the temperature. In Eq. (77) it was supposed that N_1 and N_2 Matsubara-poles in the upper and lower semi-plane lie within the contour C, respectively. Equation (77) can be rearranged as follows

$$i\frac{f(\varepsilon_n)}{\varepsilon_n - \varepsilon_m + \hbar\omega + i\delta} = -\frac{1}{2\pi}\oint_C dz \frac{f(z)}{(z-\varepsilon_n)(z-\varepsilon_m + \hbar\omega + i\delta)}$$

$$+ i\frac{\delta_T}{\pi}\sum_{k=-N_2+1}^{N_1}\frac{1}{(z_k-\varepsilon_n)(z_k-\varepsilon_m + \hbar\omega + i\delta)} \tag{78}$$

Similarly, by choosing contour C' the following expression,

$$-i\frac{f(\varepsilon_m)}{\varepsilon_n - \varepsilon_m + \hbar\omega + i\delta} = \frac{1}{2\pi}\oint_{C'} dz \frac{f(z)}{(z-\varepsilon_m)(z-\varepsilon_n - \hbar\omega - i\delta)}$$

$$+ i\frac{\delta_T}{\pi}\sum_{k=-N_1+1}^{N_2}\frac{1}{(z_k-\varepsilon_m)(z_k-\varepsilon_n - \hbar\omega - i\delta)} \tag{79}$$

can be derived. Deforming the contours such that the real axis is crossed at ∞ and $-\infty$, $\Sigma_{\mu\nu}(\mathbf{q}, \varpi)$ can be expressed as

$$\Sigma_{\mu\nu}(\mathbf{q}, \varpi) = -\frac{1}{2\pi V}\left\{\oint_C dz\, f(z)\sum_{mn}\frac{J_\mu^{nm}(\mathbf{q})J_\nu^{mn}(-\mathbf{q})}{(z-\varepsilon_n)(z-\varepsilon_m + \hbar\omega + i\delta)}\right.$$

$$\left. - \oint_{C'} dz\, f(z)\sum_{mn}\frac{J_\mu^{nm}(\mathbf{q})J_\nu^{mn}(-\mathbf{q})}{(z-\varepsilon_m)(z-\varepsilon_n - \hbar\omega - i\delta)}\right\}$$

$$+ i\frac{\delta_T}{\pi V}\left\{\sum_{k=-N_2+1}^{N_1}\sum_{mn}\frac{J_\mu^{nm}(\mathbf{q})J_\nu^{mn}(-\mathbf{q})}{(z_k-\varepsilon_n)(z_k-\varepsilon_m + \hbar\omega + i\delta)}\right.$$

$$\left. + \sum_{k=-N_1+1}^{N_2}\sum_{mn}\frac{J_\mu^{nm}(\mathbf{q})J_\nu^{mn}(-\mathbf{q})}{(z_k-\varepsilon_m)(z_k-\varepsilon_n - \hbar\omega - i\delta)}\right\} \tag{80}$$

Consider now the resolvent of the unperturbed Hamilton operator, i.e., of the Kohn-Sham Hamiltonian,

$$\widehat{G}(z) = (z\widehat{I} - \widehat{H})^{-1} \tag{81}$$

and its adjoint,

$$\widehat{G}(z)^\dagger = (z^*\widehat{I} - \widehat{H})^{-1} = \widehat{G}(z^*) \tag{82}$$

$$\widehat{G}(z) = \sum_n \frac{|n\rangle\langle n|}{z - \varepsilon_n} \tag{83}$$

it is straightforward to rewrite Eq. (80) as

$$\Sigma_{\mu\nu}(\mathbf{q}, \varpi) = -\frac{1}{2\pi V}\left\{\oint_C dz\, f(z)\, Tr(\widehat{J}_\mu(\mathbf{q})\widehat{G}(z+\hbar\omega+i\delta)\widehat{J}_\nu(-\mathbf{q})\widehat{G}(z))\right.$$

$$\left. - \oint_{C'} dz\, f(z)\, Tr(\widehat{J}_\mu(\mathbf{q})\widehat{G}(z)\widehat{J}_\nu(-\mathbf{q})\widehat{G}(z-\hbar\omega-i\delta))\right\}$$

$$+ i\frac{\delta_T}{\pi V}\left\{\sum_{k=-N_2+1}^{N_1} Tr(\widehat{J}_\mu(\mathbf{q})\widehat{G}(z_k+\hbar\omega+i\delta)\widehat{J}_\nu(-\mathbf{q})\,\widehat{G}(z_k))\right.$$

$$\left. + \sum_{k=-N_1+1}^{N_2} Tr(\widehat{J}_\mu(\mathbf{q})\widehat{G}(z_k)\widehat{J}_\nu(-\mathbf{q})\widehat{G}(z_k-\hbar\omega-i\delta))\right\} \tag{84}$$

Introducing for matters of convenience the quantity,

$$\widetilde{\Sigma}_{\mu\nu}(\mathbf{q}; z_1, z_2) = -\frac{1}{2\pi V} Tr(\widehat{J}_\mu(\mathbf{q})\widehat{G}(z_1)\widehat{J}_\nu(-\mathbf{q})\widehat{G}(z_2)) \tag{85}$$

$$\widetilde{\Sigma}_{\nu\mu}(-\mathbf{q}; z_2, z_1) = \widetilde{\Sigma}_{\mu\nu}(\mathbf{q}; z_1, z_2),$$

$$\widetilde{\Sigma}_{\mu\nu}(\mathbf{q}; z_1^*, z_2^*) = \widetilde{\Sigma}_{\nu\mu}(\mathbf{q}; z_1, z_2)^* = \widetilde{\Sigma}_{\mu\nu}(-\mathbf{q}; z_2, z_1)^* \tag{86}$$

because of the reflection symmetry for the contours C and C', Eq. (84) can be written as

$$\Sigma_{\mu\nu}(\mathbf{q}, \varpi) = \oint_C dz\, f(z)\, \widetilde{\Sigma}_{\mu\nu}(\mathbf{q}; z + \hbar\omega + i\delta, z) - \left(\oint_C dz\, f(z)\, \widetilde{\Sigma}_{\mu\nu}(-\mathbf{q}; z - \hbar\omega + i\delta, z)\right)^*$$

$$- 2i\delta_T \sum_{k=-N_2+1}^{N_1} \left(\widetilde{\Sigma}_{\mu\nu}(\mathbf{q}; z_k + \hbar\omega + i\delta, z_k) + \widetilde{\Sigma}_{\mu\nu}(-\mathbf{q}; z_k - \hbar\omega + i\delta, z_k)^*\right) \tag{87}$$

2.3.5. Integration Along the Real Axis: The Limit of Zero Lifetime Broadening

Deforming the contour C to the real axis such that the contributions from the Matsubara poles vanish and using the relations in Eq. (86), Eq. (87) trivially reduces to

$$\Sigma_{\mu\nu}(\mathbf{q}, \varpi) = \int_{-\infty}^{\infty} d\varepsilon\, f(\varepsilon)\{\widetilde{\Sigma}_{\mu\nu}(\mathbf{q}; \varepsilon + \hbar\omega + i\delta, \varepsilon + i0) - \widetilde{\Sigma}_{\mu\nu}(-\mathbf{q}; \varepsilon + \hbar\omega + i\delta, \varepsilon - i0)\}$$

$$- \int_{-\infty}^{\infty} d\varepsilon\, f(\varepsilon)\{\widetilde{\Sigma}_{\mu\nu}(\mathbf{q}; \varepsilon - i0, \varepsilon - \hbar\omega - i\delta) - \widetilde{\Sigma}_{\mu\nu}(-\mathbf{q}; \varepsilon + i0, \varepsilon - \hbar\omega - i\delta)\} \tag{88}$$

or, by inserting the definition of $\widetilde{\Sigma}_{\mu\nu}(\mathbf{q}; z_1, z_2)$,

$$\Sigma_{\mu\nu}(\mathbf{q}, \varpi) = -\frac{1}{2\pi V} \int_{-\infty}^{\infty} d\varepsilon\, f(\varepsilon)\{Tr(\widehat{J}_\mu(\mathbf{q})\widehat{G}(\varepsilon + \hbar\omega + i\delta)\widehat{J}_\nu(-\mathbf{q})\widehat{G}^+(\varepsilon))$$

$$- Tr(\widehat{J}_\mu(-\mathbf{q})\widehat{G}(\varepsilon + \hbar\omega + i\delta)\widehat{J}_\nu(\mathbf{q})\widehat{G}^-(\varepsilon))$$

$$- Tr(\widehat{J}_\mu(\mathbf{q})\widehat{G}^-(\varepsilon)\widehat{J}_\nu(-\mathbf{q})\widehat{G}(\varepsilon - \hbar\omega - i\delta))$$

$$+ Tr(\widehat{J}_\mu(-\mathbf{q})\widehat{G}^+(\varepsilon)\widehat{J}_\nu(\mathbf{q})\widehat{G}(\varepsilon - \hbar\omega - i\delta))\} \tag{89}$$

where $\widehat{G}^+(\varepsilon)$ and $\widehat{G}^-(\varepsilon)$ are the so-called up- and down-side limits of the resolvent

$$\widehat{G}^\pm(\varepsilon) = \lim_{\theta\to+0} \widehat{G}(\varepsilon \pm i\theta), \quad \widehat{G}^\pm(\varepsilon)^\dagger = \widehat{G}^\mp(\varepsilon) \tag{90}$$

By taking the limit $\delta \to 0$, Eq. (89) reduces to

$$\Sigma_{\mu\nu}(\mathbf{q}, \omega) = -\frac{1}{2\pi V} \int_{-\infty}^{\infty} d\varepsilon\, f(\varepsilon)\{Tr(\widehat{J}_\mu(\mathbf{q})\widehat{G}^+(\varepsilon + \hbar\omega)\widehat{J}_\nu(-\mathbf{q})\widehat{G}^+(\varepsilon))$$

$$- Tr(\widehat{J}_\mu(-\mathbf{q})\widehat{G}^+(\varepsilon + \hbar\omega)\widehat{J}_\nu(\mathbf{q})\widehat{G}^-(\varepsilon))$$

$$- Tr(\widehat{J}_\mu(\mathbf{q})\widehat{G}^-(\varepsilon)\widehat{J}_\nu(-\mathbf{q})\widehat{G}^-(\varepsilon - \hbar\omega))$$

$$+ Tr(\widehat{J}_\mu(-\mathbf{q})\widehat{G}^+(\varepsilon)\widehat{J}_\nu(\mathbf{q})\widehat{G}^-(\varepsilon - \hbar\omega))\} \tag{91}$$

which for $\mathbf{q} = 0$ yields

$$\Sigma_{\mu\nu}(\omega) = -\frac{1}{2\pi V} \int_{-\infty}^{\infty} d\varepsilon\, f(\varepsilon)\{Tr(\widehat{J}_\mu \widehat{G}^+(\varepsilon + \hbar\omega)\widehat{J}_\nu[\widehat{G}^+(\varepsilon) - G^-(\varepsilon)]) \tag{92}$$

$$+ Tr(\widehat{J}_\mu[\widehat{G}^+(\varepsilon) - G^-(\varepsilon)]\widehat{J}_\nu \widehat{G}^-(\varepsilon - \hbar\omega))\} \tag{93}$$

2.3.6. The Static Limit

In order to obtain the correct zero-frequency conductivity tensor, Eq. (89) has to be used in Eq. (68). Making use of the analyticity of the Green functions in the upper and lower complex semiplanes this then leads to the famous *Kubo-Luttinger formula* [5, 6],

$$
\sigma_{\mu\nu} = -\frac{\hbar}{2\pi V} \int_{-\infty}^{\infty} d\varepsilon\, f(\varepsilon)
$$
$$
\times Tr\left(\widehat{J}_\mu \frac{\partial \widehat{G}^+(\varepsilon)}{\partial \varepsilon} \widehat{J}_\nu [\widehat{G}^+(\varepsilon) - \widehat{G}^-(\varepsilon)] - \widehat{J}_\mu [\widehat{G}^+(\varepsilon) - \widehat{G}^-(\varepsilon)] \widehat{J}_\nu \frac{\partial \widehat{G}^-(\varepsilon)}{\partial \varepsilon} \right) \quad (94)
$$

Integrating by parts yields

$$
\sigma_{\mu\nu} = -\int_{-\infty}^{\infty} d\varepsilon \frac{df(\varepsilon)}{d\varepsilon} S_{\mu\nu}(\varepsilon) \quad (95)
$$

with

$$
S_{\mu\nu}(\varepsilon) = -\frac{\hbar}{2\pi V} \int_{-\infty}^{\varepsilon} d\varepsilon'
$$
$$
\times Tr\left(\widehat{J}_\mu \frac{\partial \widehat{G}^+(\varepsilon')}{\partial \varepsilon'} \widehat{J}_\nu [\widehat{G}^+(\varepsilon') - \widehat{G}^-(\varepsilon')] - \widehat{J}_\mu [\widehat{G}^+(\varepsilon') - \widehat{G}^-(\varepsilon')] \widehat{J}_\nu \frac{\partial \widehat{G}^-(\varepsilon')}{\partial \varepsilon'} \right) \quad (96)
$$

which has the meaning of a zero-temperature, energy dependent conductivity. For $T = 0$, $\sigma_{\mu\nu}$ is obviously given by

$$
\sigma_{\mu\nu} = S_{\mu\nu}(E_F) \quad (97)
$$

A numerically tractable expression can be obtained only for the *diagonal elements of the conductivity tensor*, the so-called *Kubo-Greenwood formula* [7, 8] for the dc-conductivity at finite temperatures,

$$
\sigma_{\mu\mu} = -\frac{\hbar}{4\pi V} \int_{-\infty}^{\infty} d\varepsilon \left(-\frac{df(\varepsilon)}{d\varepsilon} \right) Tr(\widehat{J}_\mu [\widehat{G}^+(\varepsilon) - \widehat{G}^-(\varepsilon)] \widehat{J}_\mu [\widehat{G}^+(\varepsilon) - \widehat{G}^-(\varepsilon)]) \quad (98)
$$

which at $T = 0$ temperature obviously can be written as

$$
\sigma_{\mu\mu} = -\frac{\hbar}{4\pi V} Tr(\widehat{J}_\mu [\widehat{G}^+(E_F) - \widehat{G}^-(E_F)] \widehat{J}_\mu [\widehat{G}^+(E_F) - \widehat{G}^-(E_F)])
$$
$$
= \frac{\hbar}{\pi V} Tr(\widehat{J}_\mu \mathrm{Im}\, \widehat{G}^+(E_F) \widehat{J}_\mu \mathrm{Im}\, \widehat{G}^+(E_F)) \quad (99)
$$

Recalling finally the spectral resolution of the resolvent,

$$
\mathrm{Im}\, \widehat{G}^+(\varepsilon) = -\pi \sum_n |n\rangle\langle n| \delta(\varepsilon - \varepsilon_n) \quad (100)
$$

it is easy to see that Eq. (99) is identical with the original *Greenwood equation* [7],

$$
\sigma_{\mu\mu} = \frac{\pi\hbar}{V} \sum_{nm} J_\mu^{nm} J_\mu^{mn} \delta(E_F - \varepsilon_n) \delta(E_F - \varepsilon_m) \quad (101)
$$

Equation (94), however, can also be reformulated as follows,

$$
\sigma_{\mu\nu} = \frac{\hbar}{2\pi V} \int_{-\infty}^{\infty} d\varepsilon\, f(\varepsilon)\, Tr\left(\widehat{J}_\mu \frac{d\widehat{G}^+(\varepsilon)}{d\varepsilon} \widehat{J}_\nu \widehat{G}^-(\varepsilon) + \widehat{J}_\mu \widehat{G}^+(\varepsilon) \widehat{J}_\nu \frac{d\widehat{G}^-(\varepsilon)}{d\varepsilon} \right)
$$
$$
- \frac{\hbar}{2\pi V} \int_{-\infty}^{\infty} d\varepsilon\, f(\varepsilon)\, Tr\left(\widehat{J}_\mu \frac{d\widehat{G}^+(\varepsilon)}{d\varepsilon} \widehat{J}_\nu \widehat{G}^+(\varepsilon) + \widehat{J}_\mu \widehat{G}^-(\varepsilon) \widehat{J}_\nu \frac{d\widehat{G}^-(\varepsilon)}{d\varepsilon} \right)
$$
$$
= \frac{\hbar}{2\pi V} \int_{-\infty}^{\infty} d\varepsilon \left(-\frac{df(\varepsilon)}{d\varepsilon} \right) Tr(\widehat{J}_\mu \widehat{G}^+(\varepsilon) \widehat{J}_\nu \widehat{G}^-(\varepsilon))
$$
$$
- \frac{\hbar}{2\pi V} \int_{-\infty}^{\infty} d\varepsilon\, f(\varepsilon)\, Tr\left(\widehat{J}_\mu \frac{d\widehat{G}^+(\varepsilon)}{d\varepsilon} \widehat{J}_\nu \widehat{G}^+(\varepsilon) + \widehat{J}_\mu \widehat{G}^-(\varepsilon) \widehat{J}_\nu \frac{d\widehat{G}^-(\varepsilon)}{d\varepsilon} \right) \quad (102)
$$

namely in terms of an expression which is similar to that of Baranger and Stone [9], but clearly can be cast into a relativistic form. This expression is of practical relevance reasonable if conductances have to be calculated.

3. GREEN'S FUNCTIONS AND SCATTERING PATH OPERATORS

In the following, only a very brief summary of multiple scattering is given. For a detailed treatise on this topic, the reader is refered to a very recent book [10] by some of the authors of the current article that contains also so-called full-potential approaches not considered here.

Suppose the potential in Eq. (1) can be partitioned into non-overlapping, spherically symmetric potentials V_i, centered at lattice positions $\mathbf{R}_i$, $i = 1 \ldots N$,

$$V(\mathbf{r}) = \sum_{i=1}^{N} V_i(\mathbf{r}_i)(\mathbf{r}_i = \mathbf{r} - \mathbf{R}_i) \tag{103}$$

$$V_i(\mathbf{r}_i) = \begin{cases} V_i(r_i) & \text{if } |\mathbf{r}_i| < S_i \\ \text{constant} & \text{otherwise} \end{cases} \tag{104}$$

where N denotes the number of scatterers in the system. For non-overlapping spheres this refers to the so-called *muffin-tin* approach and S_i is called the *muffin-tin radius* of the ith sphere. In the so-called atomic sphere approximation (ASA), the spheres are chosen to have the same volume as the Wigner-Seitz cell, thus they overlap slightly, the effect of overlapping, however, is neglected. In the region between the spheres the potential is a constant, commonly set to zero.

3.1. Single-Site Scattering

In the absence of effective fields, the *Kohn-Sham-Dirac equation* is of the form [11, 12],

$$\widehat{H}|\psi\rangle = \begin{pmatrix} (V(r) + mc^2)\widehat{I}_2 & c\hat{\sigma}_r\left(\dfrac{\partial}{\partial r} + \dfrac{1}{r} - \dfrac{1}{r}\hat{\beta}\widehat{K}\right) \\ c\hat{\sigma}_r\left(\dfrac{\partial}{\partial r} + \dfrac{1}{r} - \dfrac{1}{r}\hat{\beta}\widehat{K}\right) & (V(r) - mc^2)\widehat{I}_2 \end{pmatrix} |\psi\rangle = W|\psi\rangle \tag{105}$$

where c is the speed of light, $\hat{\sigma}_r = \hat{\mathbf{r}} \cdot \hat{\boldsymbol{\sigma}}$ with $\hat{\mathbf{r}} = \mathbf{r}/|\mathbf{r}|$, W is the total energy of the particle,

$$W^2 = p^2c^2 + m^2c^4$$

with p being its momentum and

$$\widehat{K} = \hat{\boldsymbol{\sigma}} \cdot \widehat{\mathbf{L}} + \hbar\widehat{I}_2, \quad \text{and} \quad \hat{\beta} = \begin{pmatrix} \widehat{I}_1 & 0 \\ 0 & -\widehat{I}_1 \end{pmatrix} \tag{106}$$

The wavefunction $|\psi\rangle$ can be decoupled into two bi-spinors: $|\psi\rangle = |\phi, \chi\rangle$. The total angular momentum operator is defined as $\widehat{\mathbf{J}} = \widehat{\mathbf{L}} + \widehat{\mathbf{S}}$, where $\widehat{\mathbf{L}}$ is the angular momentum operator and $\widehat{\mathbf{S}} = \frac{\hbar}{2}\hat{\boldsymbol{\sigma}}$ is the spin momentum operator. The eigenfunctions of $\widehat{J}^2$ and $\widehat{J}_z$,

$$\widehat{J}^2|\phi\rangle = \hbar^2 j(j+1)|\phi\rangle, \quad \widehat{J}^2|\chi\rangle = \hbar^2 j(j+1)|\chi\rangle, \quad j = l \pm \frac{1}{2} = \frac{1}{2}, \frac{3}{2}, \frac{5}{2}, \ldots,$$

$$\widehat{J}_z|\phi\rangle = \hbar\mu|\phi\rangle, \quad \widehat{J}_z|\chi\rangle = \hbar\mu|\chi\rangle, \quad \mu = -j, \ldots, j, \tag{107}$$

$$\widehat{K}|\phi\rangle = -\hbar\kappa|\phi\rangle, \quad \widehat{K}|\chi\rangle = \hbar\kappa|\chi\rangle, \quad \kappa = \mp\left(j + \frac{1}{2}\right)$$

are the so-called spin spherical harmonics,

$$|\kappa, \mu\rangle = |Q\rangle = \sum_{s=\pm 1/2} C\left(l, j, \frac{1}{2}\Big|\mu - s, s\right)|l, \mu - s\rangle\Phi_s, \quad |-\kappa, \mu\rangle = |\overline{Q}\rangle \tag{108}$$

where the $C(l, j, 1/2 | \mu - s, s)$ denote *Clebsch-Gordan coefficients* [13], $|l, \mu - s\rangle$ *complex spherical harmonics*,

$$\langle l, \mu - s | \hat{\mathbf{r}} \rangle = Y_l^{\mu - s}(\hat{r}) \quad \text{and} \quad \langle \hat{\mathbf{r}} | l, \mu - s \rangle = Y_l^{\mu - s}(\hat{r})^*$$

and the Φ_s are the following *spinor basis functions* [11],

$$\Phi_{1/2} = \begin{pmatrix} 1 \\ 0 \end{pmatrix}, \quad \Phi_{-1/2} = \begin{pmatrix} 0 \\ 1 \end{pmatrix} \tag{109}$$

It should be noted that in the so-called weak-relativistic limit, the following approach is used,

$$\varepsilon = W - mc^2 = \sqrt{p^2 c^2 + m^2 c^4} - mc^2 \approx \frac{p^2}{2m} \ll mc^2 \tag{110}$$

3.1.1. Free-Space Green's Functions

The nonrelativistic Green's function of a free electron in angular momentum representation can be written as

$$G_0^{nr, \pm}(\varepsilon, \mathbf{r}, \mathbf{r}') = \mp i p \sum_L j_l \left(\frac{p r_<}{\hbar} \right) h_l^{\pm} \left(\frac{p r_>}{\hbar} \right) Y_L(\hat{r}) Y_L^*(\hat{r}') \tag{111}$$

where $L = (l, m)$, $r_< = \min(r, r')$, $r_> = \max(r, r')$, and $h_l^{\pm} = j_l \pm i n_l$ is a spherical Hankel function with j_l and n_l being spherical Bessel and Neumann functions, respectively [14]. In the relativistic case the Green's function of a free electron in angular momentum representation is of the form

$$G_0^r(\varepsilon, \mathbf{r}, \mathbf{r}') = -i p \frac{\varepsilon + 2mc^2}{2mc^2} \sum_Q [J_Q(\varepsilon, \mathbf{r}) H_Q^+(\varepsilon, \mathbf{r}')^\dagger \theta(r' - r) + H_Q^+(\varepsilon, \mathbf{r}) J_Q^\dagger(\varepsilon, \mathbf{r}') \theta(r - r')] \tag{112}$$

with

$$F_Q(\varepsilon, \mathbf{r}) = \begin{bmatrix} f_l \left(\dfrac{p r}{\hbar} \right) \langle Q | \hat{\mathbf{r}} \rangle \\[4mm] \dfrac{i S_\kappa p c}{\varepsilon + 2mc^2} f_{\bar{l}} \left(\dfrac{p r}{\hbar} \right) \langle \bar{Q} | \hat{\mathbf{r}} \rangle \end{bmatrix} \tag{113}$$

$$F_Q^\dagger(\varepsilon, \mathbf{r}) = \left[f_l \left(\frac{p r}{\hbar} \right) \langle \hat{\mathbf{r}} | Q \rangle, \quad \frac{-i S_\kappa p c}{\varepsilon + 2mc^2} f_{\bar{l}} \left(\frac{p r}{\hbar} \right) \langle \hat{\mathbf{r}} | \bar{Q} \rangle \right] \tag{114}$$

and

$$S_\kappa = \frac{\kappa}{|\kappa|}, \quad \bar{l} = l - S_\kappa$$

with f_l denoting spherical Bessel-, Neumann-, or Hankel functions. A general solution of Eq. (105) can be written as

$$R(\varepsilon, \mathbf{r}) = \sum_Q R_Q(\varepsilon, \mathbf{r}) = \sum_Q \begin{bmatrix} g_\kappa(\varepsilon, r) \langle Q | \hat{\mathbf{r}} \rangle \\[2mm] i f_\kappa(\varepsilon, r) \langle \bar{Q} | \hat{\mathbf{r}} \rangle \end{bmatrix} \tag{115}$$

a solution outside the bounding sphere as

$$R_Q(\varepsilon, \mathbf{r}) = J_Q(\varepsilon, \mathbf{r}) - i p \sum_{Q'} H_{Q'}^+(\varepsilon, \mathbf{r}) t_{Q'Q}(\varepsilon) \tag{116}$$

where $t_{Q'Q}(\varepsilon)$ is usually called *single-site t-matrix*,

$$t_{Q'Q}(\varepsilon) = \int_{r<S} d^3r \int_{r'<S} d^3r' \, J_{Q'}^\dagger(\varepsilon, \mathbf{r}') t(\varepsilon, \mathbf{r}', \mathbf{r}) J_Q(\varepsilon, \mathbf{r}) \tag{117}$$

which, for example, for nonmagnetic systems and $\varepsilon \geq 0$ can easily be obtained from the below matching condition

$$g_\kappa(\varepsilon, r) = \cos \delta_\kappa(\varepsilon) j_l\left(\frac{pr}{\hbar}\right) - \sin \delta_\kappa(\varepsilon) n_l\left(\frac{pr}{\hbar}\right) \tag{118}$$

$$cf_\kappa(\varepsilon, r) = pS_\kappa\left[\cos \delta_\kappa(\varepsilon) j_{\bar{l}}\left(\frac{pr}{\hbar}\right) - \sin \delta_\kappa(\varepsilon) n_{\bar{l}}\left(\frac{pr}{\hbar}\right)\right] \tag{119}$$

at the muffin-tin radius S,

$$\tan \delta_\kappa(\varepsilon) = \frac{L_\kappa(\varepsilon, S) j_l(pS/\hbar) - pS_\kappa j_{\bar{l}}(pS/\hbar)}{L_\kappa(\varepsilon, r) n_l(pS/\hbar) - pS_\kappa n_{\bar{l}}(pS/\hbar)} \tag{120}$$

$$L_\kappa(\varepsilon, S) = \frac{cf_\kappa(\varepsilon, S)}{g_\kappa(\varepsilon, S)} \tag{121}$$

3.1.2. Scattering Solutions

The so-called (regular) scattering solutions are defined as follows

$$Z(\varepsilon, \mathbf{r}) = \sum_Q Z_Q(\varepsilon, \mathbf{r}) = \sum_{Q'Q} R_{Q'}(\varepsilon, \mathbf{r}) t_{Q'Q}^{-1}(\varepsilon) \tag{122}$$

$$Z_Q(\varepsilon, \mathbf{r}) = \sum_{Q'} J_{Q'}(\varepsilon, \mathbf{r}') K_{Q'Q}^{-1}(\varepsilon) + pN_Q(\varepsilon, \mathbf{r}) \tag{123}$$

where $K_{Q'Q}(z)$ usually is termed *reactance*

$$K_{QQ'}^{-1}(\varepsilon) = t_{QQ'}^{-1}(\varepsilon) - ip\delta_{QQ'} \tag{124}$$

$$K(\varepsilon) = K^\dagger(\varepsilon) \tag{125}$$

3.2. Multiple Scattering

3.2.1. Scattering Path Operators

The angular momentum representation of the so-called scattering path operator is given by [15]

$$\tau_{QQ'}^{ij}(\varepsilon) = t_{QQ'}^i(\varepsilon)\delta_{ij} + \sum_{k \neq i}\sum_{Q_1 Q_2} t_{QQ_1}^i(\varepsilon) G_{Q_1 Q_2}^{0, ik}(\varepsilon) \tau_{Q_2 Q'}^{kj}(\varepsilon) \tag{126}$$

where the relativistic structure constants

$$G_{QQ'}^{0, ij}(\varepsilon) = \frac{\varepsilon + 2mc^2}{2mc^2}\sum_s C\left(l, j, \frac{1}{2}\bigg| \mu - s, s\right) G_{LL'}^{0, ij}(\varepsilon) C\left(l', j', \frac{1}{2}\bigg| \mu' - s, s\right) \tag{127}$$

are obtained from the nonrelativistic ones

$$G_0^{nr}(\varepsilon, \mathbf{r}_i + \mathbf{R}_i, \mathbf{r}_j' + \mathbf{R}_j) = \sum_{L, L'} j_L(\varepsilon, \mathbf{r}_i) G_{LL'}^{0, ij}(\varepsilon) j_{L'}^\times(\varepsilon, \mathbf{r}_j') \tag{128}$$

In here, the notation $G_{LL'}^{0, ij}(\varepsilon) = G_{LL'}^0(\varepsilon, \mathbf{R}_j - \mathbf{R}_i)$ is applied, $\mathbf{R}_i$ and $\mathbf{R}_j$ denoting the position vectors of sites i and j, and $t_{QQ'}^i(\varepsilon)$ refers to the t-matrix at site $\mathbf{R}_i$, and

$$G_{LL'}^0(\varepsilon, \mathbf{r}) = -4\pi i^{(l-l'+1)} p \sum_{L''} C_{LL''}^{L'} i^{-l''} h_{L''}(\varepsilon, \mathbf{r}) \tag{129}$$

$$C_{LL''}^{L'} = \int d\hat{\mathbf{r}} Y_L(\hat{r}) Y_{L'}^*(\hat{r}) Y_{L''}(\hat{r}) \tag{130}$$

$$j_L(\varepsilon, \mathbf{r}) \equiv j_l\left(\frac{pr}{\hbar}\right) Y_L(\hat{r}), \quad j_L^\times(\varepsilon, \mathbf{r}) \equiv j_l\left(\frac{pr}{\hbar}\right) Y_L^*(\hat{r}) \tag{131}$$

where the $C_{LL''}^{L'}$ are the so-called Gaunt coefficients.

3.2.2. Green's Functions

The Green's function in the case of an ensemble of scatterers can be defined in terms of the scattering path operator and scattering solutions as

$$
G(\varepsilon, \mathbf{r}_i, \mathbf{r}'_j) = \sum_{Q, Q'} \left[Z_Q^i(\varepsilon, \mathbf{r}_i) \tau_{QQ'}^{ij}(\varepsilon) Z_{Q'}^j(\varepsilon, \mathbf{r}'_j)^\dagger - \delta_{ij} \delta_{QQ'} (\theta(r_i - r'_i) Z_Q^i(\varepsilon, \mathbf{r}'_i) I_{Q'}^i(\varepsilon, \mathbf{r}_i)^\dagger \right.
$$

$$
\left. + \theta(r'_i - r_i) I_Q^i(\varepsilon, \mathbf{r}'_i) Z_{Q'}^i(\varepsilon, \mathbf{r}_i)^\dagger) \right] \tag{132}
$$

where $Z_Q^i(\varepsilon, \mathbf{r})$ and $I_Q^i(\varepsilon, \mathbf{r})$ denote the regular and irregular scattering solutions of the Dirac equation in cell i and—as should be recalled—at the muffin-tin radius of the ith cell (S_i) the following relations have to be satisfied,

$$
Z_Q^i(\varepsilon, S_i) = \sum_{Q'} (t_{QQ'}^i)^{-1} J_{Q'}(\varepsilon, S_i) - ip H_Q^+(\varepsilon, S_i) \tag{133}
$$

$$
I_Q^i(\varepsilon, S_i) = J_Q(\varepsilon, S_i) \tag{134}
$$

3.3. KKR Method for Layered Systems

Layered systems are systems with (at least) two-dimensional translational symmetry. In the case of a surface or an interface, the translational symmetry is "broken" along the direction "perpendicular" to the plane. Suppose such a layered system corresponds to a parent infinite (three-dimensional periodic) system consisting of a simple lattice with only one atom per unit cell, then any lattice site $\mathbf{R}_{pi}$ can be written as

$$
\mathbf{R}_{pi} = \mathbf{C}_p + \mathbf{T}_i; \qquad \mathbf{T}_i \in L_2 \tag{135}
$$

where $\mathbf{C}_p$ is the "spanning vector" of a particular layer p and the two-dimensional (real) lattice is denoted by $L_2 = \{\mathbf{T}_i\}$ with in-plane lattice vectors $\mathbf{T}_i$ and where the corresponding set of indices is $I(L_2)$. It should be noted that $\mathbf{C}_p$ not necessarily has to be perpendicular to the planes of atoms, e.g., in a body centered cubic (BCC) lattice for (001)-planes $\mathbf{C}_p = p \cdot a \cdot (\frac{1}{2}, \frac{1}{2}, \frac{1}{2})$, where a is the three-dimensional lattice constant.

The real-space structure constants are now defined by

$$
\underline{G}_0^{ij}(\varepsilon) = \underline{G}_0(\varepsilon, \mathbf{R}_{pi} - \mathbf{R}_{qj}) = \underline{G}_0(\varepsilon, \mathbf{C}_p + \mathbf{T}_i - \mathbf{C}_q - \mathbf{T}_j) = \widehat{\underline{G}}_0^{pq}(\varepsilon, \mathbf{T}_i - \mathbf{T}_j)
$$

$$
= \frac{1}{\Omega_{BZ}} \int_{BZ} d^2 k_\parallel \widehat{\underline{G}}_0^{pq}(\varepsilon, \mathbf{k}_\parallel) e^{-i\mathbf{k}_\parallel \cdot (\mathbf{T}_i - \mathbf{T}_j)} \tag{136}
$$

where Ω_{BZ} denotes the volume (area) of the two-dimensional Brillouin zone, and the symbol "hat" denotes a layer-indexed quantity; the two-dimensional lattice Fourier transform of the "reciprocal" structure constants is simply given by

$$
\widehat{\underline{G}}_0^{pq}(\varepsilon, \mathbf{k}_\parallel) = \sum_{\mathbf{T}_i} \widehat{\underline{G}}_0^{pq}(\varepsilon, \mathbf{T}_i) e^{i\mathbf{k}_\parallel \cdot \mathbf{T}_i} \tag{137}
$$

Introducing the below matrix notation,

$$
\underline{\hat{t}}(\varepsilon) = \{\hat{\underline{t}}_p(\varepsilon) \delta_{pq}\}, \quad \widehat{\underline{G}}_0(\varepsilon, \mathbf{k}_\parallel) = \{\widehat{\underline{G}}_0^{pq}(\varepsilon, \mathbf{k}_\parallel)\}, \quad \underline{\hat{\tau}}(\varepsilon, \mathbf{k}_\parallel) = \{\hat{\underline{\tau}}_{pq}(\varepsilon, \mathbf{k}_\parallel)\} \tag{138}
$$

the so-called KKR (Korringa-Kohn-Rostoker) equation can be written as

$$
\underline{\hat{\tau}}(\varepsilon, \mathbf{k}_\parallel) = \left(\underline{\hat{t}}^{-1}(\varepsilon) - \widehat{\underline{G}}_0(\varepsilon, \mathbf{k}_\parallel) \right)^{-1} \tag{139}
$$

3.4. The Screened KKR Method (SKKR)

For systems containing several atoms per unit cell as well as for layered structures severe computational difficulties arise from the long range behavior of the structure constants. For such systems, tight-binding (TB) methods seem to be better suited. However, it can be shown

that by applying a so-called screening transformation, the KKR-method can be transformed into a TB form [16–18]. In Ref. [17], for example, a reference system is suggested with a constant repulsive potential V^r, defined within non-overlapping muffin-tin spheres and zero otherwise. In the following, r-indexed quantities refer to the reference system and quantities without such an index to those of the physical system, the corresponding *Green's function matrices* being defined by the below Dyson equations

$$\underline{\underline{G}}(\varepsilon) = \underline{\underline{G}}_0(\varepsilon)(\underline{\underline{I}} - \underline{\underline{t}}(\varepsilon)\underline{\underline{G}}_0(\varepsilon))^{-1}, \quad \underline{\underline{G}}^r(\varepsilon) = \underline{\underline{G}}_0(\varepsilon)(\underline{\underline{I}} - \underline{\underline{t}}^r(\varepsilon)\underline{\underline{G}}_0(\varepsilon))^{-1} \tag{140}$$

Furthermore, in defining the difference of the inverse of the t-matrices as

$$\underline{\underline{t}}_\Delta(\varepsilon) = \underline{\underline{t}}(\varepsilon) - \underline{\underline{t}}^r(\varepsilon) \tag{141}$$

and the screened scattering path operator as

$$\underline{\underline{\tau}}_\Delta(\varepsilon) = \left(\underline{\underline{t}}_\Delta^{-1}(\varepsilon) - \underline{\underline{G}}^r(\varepsilon) \right)^{-1} \tag{142}$$

the unscreened (physical) scattering path operator can be calculated from the screened one by using the following invariance property [17]

$$\underline{\underline{G}}(\varepsilon) = \underline{\underline{t}}^{-1}(\varepsilon)\underline{\underline{\tau}}(\varepsilon)\underline{\underline{t}}^{-1}(\varepsilon) - \underline{\underline{t}}^{-1}(\varepsilon) = \underline{\underline{t}}_\Delta^{-1}(\varepsilon)\underline{\underline{\tau}}_\Delta(\varepsilon)\underline{\underline{t}}_\Delta^{-1}(\varepsilon) - \underline{\underline{t}}_\Delta^{-1}(\varepsilon) \tag{143}$$

$$\underline{\underline{\tau}}(\varepsilon) = \left[\underline{\underline{I}} - \underline{\underline{t}}^r(\varepsilon)\underline{\underline{t}}^{-1}(\varepsilon) \right]\underline{\underline{\tau}}_\Delta(\varepsilon)\left[\underline{\underline{I}} - \underline{\underline{t}}^{-1}(\varepsilon)\underline{\underline{t}}^r(\varepsilon) \right] + \left[\underline{\underline{t}}^r(\varepsilon) - \underline{\underline{t}}^r(\varepsilon)\underline{\underline{t}}^{-1}(\varepsilon)\underline{\underline{t}}^r(\varepsilon) \right] \tag{144}$$

In the two-dimensional lattice Fourier transform of the screened scattering path operator,

$$\hat{\underline{\tau}}_{\Delta,pq}(\varepsilon, \mathbf{k}_\parallel) = \left\{ \left((\hat{\underline{t}}_\Delta)^{-1}(\varepsilon) - \hat{\underline{G}}^r(\varepsilon, \mathbf{k}_\parallel) \right)^{-1} \right\}_{pq} \tag{145}$$

however—because of the screening—$\widehat{G}^r$ is of block-tridiagonal form, the blocks being related to so-called principal layers that contain n atomic layers ($n \geq 3$). If these layers form the top of a semi-infinite bulk (substrate) or are situated between two semi-infinite bulk systems, a so-called surface Green function method [16] has to be applied to ensure proper boundary conditions. The real-space physical τ-matrix is then obtained first by performing the following Brillouin zone integral,

$$\underline{\tau}_\Delta(\varepsilon, \mathbf{R}_{pi} - \mathbf{R}_{qj}) = \frac{1}{\Omega_{BZ}} \int_{BZ} d^2 k_\parallel \hat{\underline{\tau}}_{\Delta,pq}(\varepsilon, \mathbf{k}_\parallel)e^{-i\mathbf{k}_\parallel \cdot (\mathbf{T}_i - \mathbf{T}_j)} \tag{146}$$

and subsequent use of the transformation defined in Eq. (144). It should be noted that in principle for a two-dimensional translational invariant medium the physical real space τ-matrix is in principle defined by

$$\underline{\tau}^{pi,qj}(\varepsilon) = \frac{1}{\Omega_{BZ}} \int_{BZ} d^2 k_\parallel \hat{\underline{\tau}}^{pq}(\varepsilon, \mathbf{k}_\parallel)e^{-i\mathbf{k}_\parallel \cdot (\mathbf{T}_i - \mathbf{T}_j)} \tag{147}$$

3.5. The Embedding Technique

A finite *cluster* is defined as a geometrical arrangement of a set of scatterers. Let $\mathscr{C}$ denote the set of the position vectors of sites in the cluster,

$$\mathscr{C} \equiv \{\mathbf{R}_i\}, \quad i = 1, \ldots, N \tag{148}$$

where N is the number of atoms in the cluster, and C_N a corresponding set of site-indices

$$C_N \equiv \{i | \mathbf{R}_i \in \mathscr{C}, \quad i = 1, \ldots, N\} \tag{149}$$

Because for the host system (*substrate*) the potential is given by

$$V^{\text{host}}(\mathbf{r}) = \sum_i V_i^{\text{host}}(\mathbf{r}_i) \tag{150}$$

and for an *embedded cluster* by

$$V^{\text{clus}}(\mathbf{r}) = \sum_i V_i^{\text{clus}}(\mathbf{r}_i), \quad V_i^{\text{clus}}(\mathbf{r}_i) = \begin{cases} V_i^{\text{host}}(\mathbf{r}_i) & \text{if } i \notin C_N \\ V_i^{\text{imp}}(\mathbf{r}_i) & \text{if } i \in C_N \end{cases} \tag{151}$$

the single site t-matrices of the perturbed system are of the form,

$$\underline{t}_{\text{clus}}^i(\varepsilon) = \begin{cases} \underline{t}_{\text{host}}^i(\varepsilon) & \text{if } i \notin C_N \\ \underline{t}_{\text{imp}}^i(\varepsilon) & \text{if } i \in C_N \end{cases} \tag{152}$$

It is important to emphasize that by performing real space embedding, a cluster usually contains the investigated impurity atoms, some sites from the host material (and empty spheres (vacuum) in the case of a surface or a nanocontact). In principle according to the above classification all V_i^{imp}, $\underline{t}_{\text{imp}}^i$ are different.

The KKR-equation for the unperturbed and perturbed systems are then given by,

$$\underline{\underline{\tau}}_{\text{host}}^{-1}(\varepsilon) = \underline{\underline{t}}_{\text{host}}^{-1}(\varepsilon) - \underline{\underline{G}}_0(\varepsilon), \quad \underline{\underline{\tau}}_{\text{clus}}^{-1}(\varepsilon) = \underline{\underline{t}}_{\text{clus}}^{-1}(\varepsilon) - \underline{\underline{G}}_0(\varepsilon) \tag{153}$$

respectively, with

$$\underline{\tau}(\varepsilon) = \{\underline{\tau}^{ij}(\varepsilon)\}, \quad \underline{\tau}^{ij}(\varepsilon) = \{\tau_{QQ'}^{ij}(\varepsilon)\}, \quad \underline{t}(\varepsilon) = \{\underline{t}^i(\varepsilon)\delta_{ij}\}, \quad \underline{t}^i(\varepsilon) = \{t_{QQ'}^i(\varepsilon)\} \tag{154}$$

Defining the following quantities

$$\Delta \underline{\underline{t}}^{-1}(\varepsilon) = \underline{\underline{t}}_{\text{host}}^{-1}(\varepsilon) - \underline{\underline{t}}_{\text{clus}}^{-1}(\varepsilon) = \{\Delta \underline{t}^i(\varepsilon)^{-1}\delta_{ij}\}$$

$$\Delta \underline{t}^i(\varepsilon)^{-1} = \begin{cases} 0, & \text{if } i \notin C_N \\ \underline{t}_{\text{host}}^i(\varepsilon)^{-1} - \underline{t}_{\text{imp}}^i(\varepsilon)^{-1}, & \text{if } i \in C_N \end{cases} \tag{155}$$

from Eq. (153), one then obtains

$$\begin{aligned} \underline{\underline{\tau}}_{\text{clus}}^{-1}(\varepsilon) &= \underline{\underline{\tau}}_{\text{host}}^{-1}(\varepsilon) - \Delta \underline{\underline{t}}^{-1}(\varepsilon) \\ &= \left[\underline{\underline{I}} - \Delta \underline{\underline{t}}^{-1}(\varepsilon)\underline{\underline{\tau}}_{\text{host}}(\varepsilon)\right]\underline{\underline{\tau}}_{\text{host}}^{-1}(\varepsilon) \\ &= \underline{\underline{\tau}}_{\text{host}}^{-1}(\varepsilon)\left[\underline{\underline{I}} - \underline{\underline{\tau}}_{\text{host}}(\varepsilon)\Delta \underline{\underline{t}}^{-1}(\varepsilon)\right] \end{aligned} \tag{156}$$

which inverted finally leads to the below *embedding equation*,

$$\underline{\underline{\tau}}_{\text{clus}}(\varepsilon) = \underline{\underline{\tau}}_{\text{host}}(\varepsilon)\left[\underline{\underline{I}} - \Delta \underline{\underline{t}}^{-1}(\varepsilon)\underline{\underline{\tau}}_{\text{host}}(\varepsilon)\right]^{-1} = \left[\underline{\underline{I}} - \underline{\underline{\tau}}_{\text{host}}(\varepsilon)\Delta \underline{\underline{t}}^{-1}(\varepsilon)\right]^{-1}\underline{\underline{\tau}}_{\text{host}}(\varepsilon) \tag{157}$$

It should be mentioned that for a *single impurity* at site i_0 the above embedding equation reduces to

$$\begin{aligned} \underline{\tau}^{i_0,i_0}(\varepsilon) &= \underline{\tau}_{\text{host}}^{i_0,i_0}(\varepsilon)\left[\underline{\underline{I}} - \Delta \underline{t}^{i_0}(\varepsilon)^{-1}\underline{\tau}_{\text{host}}^{i_0,i_0}(\varepsilon)\right]^{-1} = \underline{\tau}_{\text{host}}^{i_0,i_0}(\varepsilon)\underline{\widetilde{D}}^{i_0}(\varepsilon) \\ &= \left[\underline{\underline{I}} - \underline{\tau}_{\text{host}}^{i_0,i_0}(\varepsilon)\Delta \underline{t}^{i_0}(\varepsilon)^{-1}\right]^{-1}\underline{\tau}_{\text{host}}^{i_0,i_0}(\varepsilon) = \underline{D}^{i_0}(\varepsilon)\underline{\tau}_{\text{host}}^{i_0,i_0}(\varepsilon) \end{aligned} \tag{158}$$

3.6. The Coherent Potential Approximation

3.6.1. Configurational Averages

Suppose a binary bulk alloy is of composition $A_c B_{1-c}$ with $c_A = c$ being the concentration of species A and $c_B = (1-c)$ the concentration of species B. Furthermore, suppose the total number of atoms is N and the number of A atoms and B atoms N_A and N_B, respectively,

$$N = N_A + N_B, \quad N_A = cN, \quad N_B = (1-c)N \tag{159}$$

A substitutional binary alloy refers to a system with no positional disorder, all atoms are placed (for matters of simplicity) in the positions of an underlying ideal simple lattice $\mathscr{L}$ which is characterized by the set of indices, $I(\mathscr{L})$. Assuming this kind of disorder, the potential can be written as

$$V(\mathbf{r}) = \sum_{i \in I(\mathscr{L})} V_i(\mathbf{r}_i - \mathbf{R}_i) \tag{160}$$

$$V_i(\mathbf{r}_i - \mathbf{R}_i) = \xi_i V_A(\mathbf{r}_i - \mathbf{R}_i) + (1 - \xi_i)V_B(\mathbf{r}_i - \mathbf{R}_i) \tag{161}$$

where ξ_i is an occupational variable such that $\xi_i = 1$ if site $\mathbf{R}_i$ is occupied by species A and $\xi_i = 0$ if this site is occupied by species B. For a completely random alloy the probability for $\xi_i = 1$ is c_A and correspondingly for $\xi_i = 0$ the probability is c_B. In Eq. (161), $V_A(\mathbf{r}_i - \mathbf{R}_i)$ and $V_B(\mathbf{r}_i - \mathbf{R}_i)$ are the individual (effective) potentials of species A and B at site $\mathbf{R}_i$, respectively. Then $\{\xi_i \mid i \in I(\mathscr{L})\}$ is one particular arrangement of atoms A and B on the positions of $\mathscr{L}$. Such an arrangement is called a *configuration*. Quite clearly for one particular configuration the Kohn-Sham equation,

$$\widehat{H}\{\xi_i\}\psi_n(\mathbf{r}, \{\xi_i\}) = \varepsilon_n\{\xi_i\}\psi_n(\mathbf{r}, \{\xi_i\}) \tag{162}$$

where $\widehat{H}$ is the Hamiltonian of the system and n labels the eigenstates, can be solved using standard techniques. Observables, however, in general do not map a particular configuration but an average over all configurations. Let $\langle A_{nn'} \rangle$ be the configurationally averaged matrix element of a Hermitian operator $\widehat{A}$. Then

$$\langle A_{nn'} \rangle = \sum_{\{\xi_i\}} P(\{\xi_i\})\langle \psi_n\{\xi_i\}|\widehat{A}|\psi_{n'}\{\xi_i\}\rangle \tag{163}$$

where $P(\{\xi_i\})$ is the microcanonical probability for a particular configuration $\{\xi_i\}$. In the above equations it was assumed that the occupational probabilities for different sites are independent from each other, that is, that

$$P(\{\xi_i\}) = \prod_i P_i(\xi_i), \quad \sum_{\xi_i = 0,\, 1} P_i(\xi_i) = 1$$
$$\langle \xi_i \rangle \equiv P_i(1) = c, \quad \langle 1 - \xi_i \rangle \equiv P_i(0) = 1 - c \tag{164}$$

Obviously the calculation of averages such in specified Eq. (163) is greatly simplified by directly calculating the configurationally averaged Green function $\langle G^+(\varepsilon, \mathbf{r}, \mathbf{r}') \rangle$ from which typical one-particle physical properties can immediately be obtained.

Restricted ensemble averages, denoted by $\langle \ldots \rangle_{(i=\alpha)}$, have the following meaning: in cell i the occupation is fixed to atom $\alpha(\alpha \in \{A, B\})$ and the averaging is restricted to all configurations for the remaining $N - 1$ sites. By using restricted ensemble averages the configurational average is partitioned into two subsets, for which the following condition has to be satisfied,

$$\langle G^+(\varepsilon, \mathbf{r}_i, \mathbf{r}_i) \rangle = \sum_{\alpha \in \{A, B\}} c_\alpha \langle G^+(\varepsilon, \mathbf{r}_i, \mathbf{r}_i) \rangle_{(i=\alpha)} \tag{165}$$

3.6.2. The CPA Single-Site Approximation

In the so-called single-site approximation to the coherent potential approximation (CPA), *short-range-order effects* are explicitly excluded. Multiple scattering effects, however, are implicitly included since the single-site approximation is based on the idea of a single scatterer immersed in an average medium, that is, on the very concept of a "mean field theory." From the definition of the scattering path operators follows that for a binary (bulk) system A_cB_{1-c} (simple lattice, one atom per unit cell) the restricted averages $\langle \underline{\tau}^{ii}(\varepsilon) \rangle_{(i=\alpha)}$, $\alpha \in \{A, B\}$, have to meet the condition,

$$c\langle \underline{\tau}^{ii}(\varepsilon) \rangle_{(i=A)} + (1 - c)\langle \underline{\tau}^{ii}(\varepsilon) \rangle_{(i=B)} = \langle \underline{\tau}^{ii}(\varepsilon) \rangle \tag{166}$$

Because (166) is valid for all site indices $i \in I(\mathscr{L})$, it is sufficient to restrict this equation to $i = 0$ (0 = origin of the underlying lattice) for a bulk, or—more general—to $i = p0$ ($p0$, origin of the pth layer, $\forall\, p$) for layered systems.

For a given set of n atomic layers, containing also disordered layers, the so-called coherent scattering path operator $\tau_c(\varepsilon)$ is given by the following two-dimensional Brillouin zone integral,

$$\underline{\tau}_c^{pi,\,qj}(\varepsilon) = \frac{1}{\Omega_{BZ}} \int_{BZ} e^{-i\mathbf{k}_{\|} \cdot (\mathbf{T}_i - \mathbf{T}_j)} \widehat{\underline{\tau}}_c^{pq}(\varepsilon, \mathbf{k}_{\|})\, d^2 k_{\|} \tag{167}$$

where pi and qj denote site i in layer p and site j in layer q, respectively. Moreover, $\widehat{\underline{\tau}}_c^{pq}(\varepsilon, \mathbf{k}_{\|})$ is the (pq)-th block of the supermatrix,

$$\widehat{\underline{\underline{\tau}}}_c(\varepsilon, \mathbf{k}_{\|}) = \left[\widehat{\underline{\underline{t}}}_c(\varepsilon)^{-1} - \widehat{\underline{\underline{G}}}(\varepsilon, \mathbf{k}_{\|}) \right]^{-1} \tag{168}$$

Equation (167) implies two–dimensional translational invariance of the coherent medium for all layers under investigation, that is, that in each layer p for the coherent single-site t-matrices the following translational invariance applies,

$$\underline{t}_c^{pi}(\varepsilon) = \underline{t}_c^{p0}(\varepsilon) = \widehat{\underline{t}}_c^{p}(\varepsilon); \qquad \forall\, i \in I(L_2) \tag{169}$$

Using again supermatrices for a better visualization,

$$\widehat{\underline{\underline{t}}}_c(\varepsilon) = \begin{pmatrix} \widehat{\underline{t}}_c^{1}(\varepsilon) & 0 & \cdots & \cdots & 0 \\ 0 & \ddots & & & \vdots \\ \vdots & & \widehat{\underline{t}}_c^{p}(\varepsilon) & & \vdots \\ \vdots & & & \ddots & 0 \\ 0 & \cdots & \cdots & 0 & \widehat{\underline{t}}_c^{n}(\varepsilon) \end{pmatrix} \tag{170}$$

and

$$\widehat{\underline{\underline{\tau}}}_c(\varepsilon) = \begin{pmatrix} & \vdots & & \vdots & \\ \cdots & \widehat{\underline{\tau}}_c^{pp}(\varepsilon) & \cdots & \widehat{\underline{\tau}}_c^{pq}(\varepsilon) & \cdots \\ & \vdots & & \vdots & \\ \cdots & \widehat{\underline{\tau}}_c^{qp}(\varepsilon) & \cdots & \widehat{\underline{\tau}}_c^{qq}(\varepsilon) & \cdots \\ & \vdots & & \vdots & \end{pmatrix} \qquad p, q = 1, \ldots, n \tag{171}$$

quite clearly, a particular element of $\widehat{\underline{\underline{\tau}}}_c(\varepsilon)$,

$$\widehat{\underline{\tau}}_c^{pq}(\varepsilon) = \underline{\tau}_c^{pi,\,qi}(\varepsilon) = \underline{\tau}_c^{p0,\,q0}(\varepsilon) = \frac{1}{\Omega_{BZ}} \int_{BZ} \widehat{\underline{\tau}}_c^{pq}(\varepsilon, \mathbf{k}_{\|})\, d^2 k_{\|} \tag{172}$$

refers then to the unit cells at the origin of L_2 in layers p and q. Suppose now, in general, the concentration for constituents A and B in layer p is denoted by $c_p^{\alpha}(p = 1, \ldots, n; \alpha \in \{A, B\})$. By defining so-called impurity matrices, see also Eq. (159), that specify a single impurity of type α in the translational invariant coherent host formed by layer p, as

$$\widehat{\underline{D}}_{\alpha}^{p}(\varepsilon) \equiv \underline{D}_{\alpha}^{p0}(\varepsilon) = \left[\underline{I} - \underline{\tau}_c^{p0,\,p0}(\varepsilon) \underline{m}_{\alpha}^{p0}(\varepsilon) \right]^{-1} \tag{173}$$

$$\widehat{\underline{\widetilde{D}}}_{\alpha}^{p}(\varepsilon) \equiv \underline{\widetilde{D}}_{\alpha}^{p0}(\varepsilon) = \left[\underline{I} - \underline{m}_{\alpha}^{p0}(\varepsilon) \underline{\tau}_c^{p0,\,p0}(\varepsilon) \right]^{-1} \tag{174}$$

with

$$m_\alpha^{p0}(\varepsilon) = \underline{m}_\alpha^{pi}(\varepsilon) = \widehat{\underline{m}}_\alpha^p(\varepsilon) = \hat{\underline{t}}_c^p(\varepsilon)^{-1} - \hat{\underline{t}}_\alpha^p(\varepsilon)^{-1}, \quad \alpha \in \{A, B\} \tag{175}$$

where $\hat{\underline{t}}_\alpha^p(\varepsilon)$ is the single-site t-matrix for constituent α in layer p, the coherent scattering path operator for the interface region, $\hat{\underline{\tau}}_c(\varepsilon)$ is obtained from the following inhomogeneous CPA condition,

$$\widehat{\underline{\tau}}_c^{pp}(\varepsilon) = \sum_{\alpha \in \{A, B\}} c_p^\alpha \langle \widehat{\underline{\tau}}^{pp}(\varepsilon) \rangle_{p, \alpha} \tag{176}$$

$$\langle \widehat{\underline{\tau}}^{pp}(\varepsilon) \rangle_{p, \alpha} = \widehat{\underline{\tau}}_\alpha^{pp}(\varepsilon) = \widehat{\underline{D}}_\alpha^P(\varepsilon) \widehat{\underline{\tau}}_c^{pp}(\varepsilon) = \widehat{\underline{\tau}}_c^{pp}(\varepsilon) \widehat{\underline{\widetilde{D}}}_\alpha^p(\varepsilon) \tag{177}$$

that is, from a condition that implies solving *simultaneously* a layer-diagonal CPA condition for layers $p = 1, \ldots, n$. Once this condition is met then translational invariance in each layer under consideration is achieved,

$$\langle \widehat{\underline{\tau}}^{pp}(\varepsilon) \rangle_{p, \alpha} \equiv \langle \underline{\tau}^{p0, p0}(\varepsilon) \rangle_{(p0=\alpha)} = \langle \underline{\tau}^{pi, pi}(\varepsilon) \rangle_{(pi=\alpha)},$$
$$\forall i \in I(L_2), \quad p = 1, \ldots, n \tag{178}$$

As before, restricted ensemble averages can be viewed as embedding an atom of type α into the two-dimensional translationally invariant coherent medium,

$$\langle \underline{\tau}^{p0, p0}(\varepsilon) \rangle_{(p0=\alpha)} = \widehat{\underline{D}}_\alpha^P(\varepsilon) \underline{\tau}_c^{p0, p0}(\varepsilon) = \underline{\tau}_c^{p0, p0}(\varepsilon) \widehat{\underline{\widetilde{D}}}_\alpha^p(\varepsilon) \tag{179}$$

Similarly, by specifying the occupation on two different sites the following restricted averages are obtained,

$$p \neq q: \langle \underline{\tau}^{pi, qj}(\varepsilon) \rangle_{(pi=\alpha, qj=\beta)} = \widehat{\underline{D}}_\alpha^p(\varepsilon) \underline{\tau}_c^{pi, qj}(\varepsilon) \widehat{\underline{\widetilde{D}}}_\beta^q(\varepsilon) \tag{180}$$

$$p = q, \quad i \neq j: = \langle \underline{\tau}^{pi, pj}(\varepsilon) \rangle_{(pi=\alpha, pj=\beta)} = \widehat{\underline{D}}_\alpha^p(\varepsilon) \underline{\tau}_c^{pi, pj}(\varepsilon) \widehat{\underline{\widetilde{D}}}_\beta^p(\varepsilon) \tag{181}$$

where $\langle \underline{\tau}_c^{pi, qj}(\varepsilon) \rangle_{(pi=\alpha, qj=\beta)}$ has the meaning that site (subcell) pi is occupied by species α and site (subcell) qj by species β.

4. A PRACTICAL GREEN'S FUNCTION FORMULATION OF ELECTRIC TRANSPORT

4.1. Nonlocal Conductivity

A practical expression for the diagonal elements of the non-local conductivity tensor can be obtained by rewriting Eq. (99) in terms of Green's functions,

$$\sigma_{\mu\mu}^{pi, qj} = -\frac{\hbar}{4\pi V_{at}} \int_{\Omega_{pi}} d^3 r_{pi} \int_{\Omega_{qj}} d^3 r'_{qj} Tr(J_\mu [G^+(E_F; \mathbf{r}_{pi}, \mathbf{r}'_{qj}) - G^-(E_F; \mathbf{r}_{pi}, \mathbf{r}'_{qj})]$$
$$\times J_\mu [G^+(E_F; \mathbf{r}'_{qj}, \mathbf{r}_{pi}) - G^-(E_F; \mathbf{r}'_{qj}, \mathbf{r}_{pi})]) \tag{182}$$

where $\mu \in \{x, y, z\}$, N_0 is the total number of sites of a system of total volume $V = N_0 V_{at}$ (assuming no lattice relaxation, thus V_{at} is the same for all sites) with $G^\pm(E_F; \mathbf{r}_{pi}, \mathbf{r}'_{qj})$ refering to the up- and down-side limits of the Green's function. The integration is carried out over the ith unit cell in layer p, Ω_{pi}, and the j-th unit cell in layer q, Ω_{qj} and Tr denotes the trace over four-component spinors (relativistic formulation). Eq. (182), can be partitioned into four parts,

$$\sigma_{\mu\mu}^{pi, qj} = \lim_{\delta \to 0} \frac{1}{4} [\tilde{\sigma}_{\mu\mu}^{pi, qj}(\varepsilon^+, \varepsilon^+) + \tilde{\sigma}_{\mu\mu}^{pi, qj}(\varepsilon^-, \varepsilon^-) - \tilde{\sigma}_{\mu\mu}^{pi, qj}(\varepsilon^+, \varepsilon^-) - \tilde{\sigma}_{\mu\mu}^{pi, qj}(\varepsilon^-, \varepsilon^+)] \tag{183}$$

each term thereof is easily expressed in terms of scattering path operators, namely

$$\tilde{\sigma}_{\mu\mu}^{pi,qj}(\varepsilon_1, \varepsilon_2) = -\frac{\hbar}{\pi V_{at}} tr\left[\underline{J}_{\mu}^{pi}(\varepsilon_2, \varepsilon_1)\underline{\tau}_{\text{clus}}^{pi,qj}(\varepsilon_1)\underline{J}_{\mu}^{qj}(\varepsilon_1, \varepsilon_2)\underline{\tau}_{\text{clus}}^{qj,pi}(\varepsilon_2)\right] \tag{184}$$

where the underlined quantities refer to angular momentum representations and

$$\varepsilon_{1,2} = \varepsilon^{\pm} = E_F \pm i\delta \tag{185}$$

In a relativistic formulation the current matrices are given by

$$\underline{J}_{\mu}^{pi}(\varepsilon_1, \varepsilon_2) = J_{\mu,QQ'}^{pi} = ec\int_{\Omega_{pi}} Z_Q^{pi}(\mathbf{r}_{pi}, \varepsilon_1)^{\dagger}\alpha_{\mu}Z_{Q'}^{pi}(\mathbf{r}_{pi}, \varepsilon_2)d^3r_{pi}, \quad Q = (\kappa, \mu) \tag{186}$$

with α_{μ} denoting Dirac matrices, while in the non-relativistic case,

$$\underline{J}_{\mu}^{pi}(\varepsilon_1, \varepsilon_2) = J_{\mu,\Lambda\Lambda'}^{pi} = \frac{e}{m}\frac{\hbar}{i}\int_{\Omega_{pi}} Z_{\Lambda}^{pi}(\mathbf{r}_{pi}, \varepsilon_1)^{\dagger}\frac{\partial}{\partial r_{pi,\mu}}Z_{\Lambda'}^{pi}(\mathbf{r}_{pi}, \varepsilon_2)d^3r_{pi}, \quad \Lambda = (l, m) \tag{187}$$

In the above equations, the $Z^{pi}(\mathbf{r}_{pi}, \varepsilon)$ are properly normalized regular scattering solutions of the radial Schrödinger or Dirac equation. It should be noted that in all examples shown further on exclusively relativistic current matrices have been used.

4.2. Nonlocal Conductivity in Disordered Systems

In order to describe substitutional binary alloys, configurational averages have to be performed in Eq. (184) [8, 19]. Omitting vertex corrections and using the single site approximation to the Coherent Potential Approximation (CPA) the site-diagonal terms are then defined as

$$\langle\tilde{\sigma}_{\mu\mu}^{pi,pi}(\varepsilon_1, \varepsilon_2)\rangle = \sum_{\alpha} c_{\alpha} tr\left[\underline{\tilde{D}}_{\alpha}^{pi}(\varepsilon_2)\underline{J}_{\mu}^{\alpha}(\varepsilon_2, \varepsilon_1)\underline{D}_{\alpha}^{pi}(\varepsilon_1)\underline{\tau}_c^{pi,pi}(\varepsilon_1)\underline{J}_{\mu}^{\alpha}(\varepsilon_1, \varepsilon_2)\tau_c^{pi,pi}(\varepsilon_2)\right] \tag{188}$$

or, by introducing the following quantity

$$\underline{\tilde{J}}_{\mu}^{pi,\alpha}(\varepsilon_1, \varepsilon_2) = \underline{\tilde{D}}_{\alpha}^{pi}(\varepsilon_1)\underline{J}_{\mu}^{\alpha}(\varepsilon_1, \varepsilon_2)\underline{D}_{\alpha}^{pi}(\varepsilon_2) \tag{189}$$

as

$$\langle\tilde{\sigma}_{\mu\mu}^{pi,pi}(\varepsilon_1, \varepsilon_2)\rangle = \sum_{\alpha} c_{\alpha} tr\left[\underline{\tilde{J}}_{\mu}^{pi,\alpha}(\varepsilon_2, \varepsilon_1)\underline{\tau}_c^{pi,pi}(\varepsilon_1)\underline{J}_{\mu}^{\alpha}(\varepsilon_1, \varepsilon_2)\tau_c^{pi,pi}(\varepsilon_2)\right] \tag{190}$$

where c_{α} denotes the (homogeneous) concentration of the α-th component, $\alpha \in \{A, B\}$, of a binary *bulk* alloy and the current matrix $\underline{J}_{\mu}^{\alpha}$ refers to species α.

For the off-site diagonal case, $(pi) \neq (qj)$, this kind of approach yields

$$\langle\tilde{\sigma}_{\mu\mu}^{pi,qj}(\varepsilon_1, \varepsilon_2)\rangle = \sum_{\alpha,\beta} c_{\alpha}c_{\beta}\, tr\left[\underline{\tilde{D}}_{\alpha}^{pi}(\varepsilon_2)\underline{J}_{\mu}^{\alpha}(\varepsilon_2, \varepsilon_1)\underline{D}_{\alpha}^{pi}(\varepsilon_1)\underline{\tau}_c^{pi,qj}(\varepsilon_1)\right.$$
$$\left. \times\ \underline{\tilde{D}}_{\beta}^{qj}(\varepsilon_1)\underline{J}_{\mu}^{\beta}(\varepsilon_1, \varepsilon_2)\underline{D}_{\beta}^{qj}(\varepsilon_2)\underline{\tau}_c^{qj,pi}(\varepsilon_2)\right] \tag{191}$$

or, in using Eq. (189),

$$\langle\tilde{\sigma}_{\mu\mu}^{pi,qj}(\varepsilon_1, \varepsilon_2)\rangle = \sum_{\alpha,\beta} c_{\alpha}c_{\beta}\, tr\left[\underline{\tilde{J}}_{\mu}^{pi,\alpha}(\varepsilon_2, \varepsilon_1)\underline{\tau}_c^{pi,qj}(\varepsilon_1)\underline{\tilde{J}}_{\mu}^{qj,\beta}(\varepsilon_1, \varepsilon_2)\underline{\tau}_c^{qj,pi}(\varepsilon_2)\right] \tag{192}$$

4.3. The "Large Cluster" Limit

If only unperturbed host atoms form the cluster then by increasing the size of the cluster the physical properties characteristic for the corresponding bulk or substrate have to be expected. A rigorous test for a *"real space formulation"* of the Kubo equation consists therefore in considering the following convergence procedure for the diagonal elements of the resistivity ρ

$$\rho_{\mu\mu} = \lim_{\delta \to 0} \rho_{\mu\mu}(r_0; \delta), \quad \rho_{\mu\mu}(r_0; \delta) = \lim_{r \to r_0} \rho_{\mu\mu}(r; \delta) \tag{193}$$

$$\rho_{\mu\mu}(r; \delta) = [\sigma^0_{\mu\mu}(r; \delta)]^{-1}, \quad \sigma^0_{\mu\mu}(r; \delta) = \sum_j \sigma^{0j}_{\mu\mu}(\delta) \tag{194}$$

where r denotes the radius of a sphere with the origin in site $i = 0$ and r_0 is an arbitrarily large radius. The summation in Eq. (194) extends over all sites circumscribed by r; δ refers to the imaginary part of the Fermi energy. In performing the $\delta \to 0$ limit at the stage of Eq. (193) actually means that the side limits in Eq. (183) are taken at the last possible step.

Shrinking the sphere to a circle within the plane of a specific layer p (e.g., surface layer), then in the $r \to \infty$ limit the following condition must be satisfied

$$\lim_{r \to \infty} \rho_{\mu\mu}(r, \delta) = \widehat{\rho}^{pp}_{\mu\mu}(\delta), \quad \widehat{\rho}^{pp}_{\mu\mu}(\delta) = \left[\widehat{\sigma}^{pp}_{\mu\mu}(\delta)\right]^{-1} \tag{195}$$

where $\widehat{\sigma}^{pp}_{\mu\mu}$ is the layer-diagonal conductivity of layer p,

$$\widehat{\sigma}^{pp}_{\mu\mu}(\delta) = \frac{1}{4}\left[\widetilde{\widehat{\sigma}}^{pp}_{\mu\mu}(\varepsilon^+, \varepsilon^+) + \widetilde{\widehat{\sigma}}^{pp}_{\mu\mu}(\varepsilon^-, \varepsilon^-) - \widetilde{\widehat{\sigma}}^{pp}_{\mu\mu}(\varepsilon^+, \varepsilon^-) - \widetilde{\widehat{\sigma}}^{pp}_{\mu\mu}(\varepsilon^-, \varepsilon^+)\right] \tag{196}$$

for which each term on the rhs of the last equation can also be calculated directly using a two-dimensional lattice Fourier transformation,

$$\widetilde{\widehat{\sigma}}^{pp}_{\mu\mu}(\varepsilon_1, \varepsilon_2) = -\frac{\hbar}{\pi V_{at}} \frac{1}{\Omega_{BZ}} \int_{BZ} d^2k_{\parallel} \, tr\left[\widehat{\underline{J}}^p_{\mu}(\varepsilon_2, \varepsilon_1)\widehat{\underline{\tau}}^{pp}(\varepsilon_1, \mathbf{k}_{\parallel})\widehat{\underline{J}}^p_{\mu}(\varepsilon_1, \varepsilon_2)\widehat{\underline{\tau}}^{pp}(\varepsilon_2, \mathbf{k}_{\parallel})\right] \tag{197}$$

Using a sphere of radius r the summation must provide in the $r \to \infty$ limit the total conductivity of the bulk system,

$$\sigma^{\text{total}}_{\mu\mu} = \lim_{\delta \to 0} \sigma^{\text{total}}_{\mu\mu}(\delta) = \lim_{\delta \to 0}\left[\lim_{r \to \infty} \sigma^0_{\mu\mu}(r, \delta)\right] \tag{198}$$

Inverting $\sigma^{\text{total}}_{\mu\mu}$, the resistivity of a bulk system is obtained, which is zero for pure metals and finite for (disordered) alloy bulk systems (the so-called residual resistivity).

Quite clearly there are more efficient methods to evaluate resistivities for bulk or layered systems by making use of three- or two-dimensional lattice Fourier transformations, respectively. However, once it comes to determine, e.g., the electric properties of magnetic islands on surfaces, these methods are no longer applicable, and one has to rely on real space approaches as presented in here. It should be noted that the results in the "large cluster" limit presented later on are only illustrations of the reliability and applicability of the real space approach to the Kubo equation.

4.4. "Residual Resistivity" for Nanostructures

If no translational symmetry is present, then in principle one has to sum over all sites including the leads, contacts, and so forth; that is,

$$\widetilde{\sigma}_{\mu\mu}(\varepsilon_1, \varepsilon_2) = \frac{1}{N_0} \sum_{i=1}^{N_0} \sum_{j=1}^{N_0} \widetilde{\sigma}^{ij}_{\mu\mu}(\varepsilon_1, \varepsilon_2) \tag{199}$$

with $N_0 \approx 10^{23}$. Here, i and j denote sites without labelling layers explicitly. As such a procedure is numerically not accessible, the following quantity can be defined,

$$\tilde{\sigma}_{\mu\mu}(\varepsilon_1, \varepsilon_2; n) = \frac{1}{n} \sum_{i=1}^{n} \sum_{j=1}^{n} \tilde{\sigma}_{\mu\mu}^{ij}(\varepsilon_1, \varepsilon_2) \tag{200}$$

with n being the number of sites in a chosen region ("cluster"). This implies, however, that the convergence properties of $\tilde{\sigma}_{\mu\mu}(\varepsilon_1, \varepsilon_2; n)$ with respect to n have to be investigated. Because clearly enough a summation over all sites including the semi-infinite substrate would yield only the resistivity of the substrate, namely zero in the case of a pure metal, a kind of "residual resistivity" for finite clusters has to be defined,

$$\rho_{\mu\mu}^{\alpha}(r) = \left[\frac{1}{n} \sum_{i \in \text{chain}} \sum_{j=1}^{N(r)} \sigma_{\mu\mu}^{ij} \right]^{-1} \tag{201}$$

where, for example, in the case of a finite chain embedded in the surface of a suitable substrate n denotes the number of atoms in the chain of type α and $N(r)$ is the number of atoms involved in the cluster (chain + substrate neighbourhood up to a chosen value r for the circumscribing sphere).

4.5. Conductances

Linear response theory applies to an arbitrary choice for the perturbating electric field because the response function is obtained in the limit of a vanishing perturbation. Consider that a constant electric field, E_z^q, pointing along the z axis, that is, normal to the planes, is applied in all cells of layer q. Denoting the z component of the current density averaged over cell i in layer p by j_z^{pi}, the microscopic Ohm's law reads as

$$j_z^{pi} = \frac{1}{V_{at}} \sum_{j} \sigma_{zz}^{pi, qj} E_z^q \tag{202}$$

where V_{at} is the volume of the unit cell in layer p. Note, that in neglecting lattice relaxations, V_{at} is uniform for the whole system. According to the Kubo-Greenwood equation at zero temperature, see Eq. (99), the zz component of the non-local conductivity tensor $\sigma_{zz}^{pi, qj}$ can be written as

$$\sigma_{zz}^{pi, qj} = -\frac{\hbar}{4\pi} \int_{\Omega_{pi}} d^3 r_{pi} \int_{\Omega_{qj}} d^3 r'_{qj} \, Tr\big(J_z[G^+(E_F; \mathbf{r}_{pi}, \mathbf{r}'_{qj}) - G^-(E_F; \mathbf{r}_{pi}, \mathbf{r}'_{qj})]$$
$$\times J_z[G^+(E_F; \mathbf{r}'_{qj}, \mathbf{r}_{pi}) - G^-(E_F; \mathbf{r}'_{qj}, \mathbf{r}_{pi})]\big) \tag{203}$$

However, the total current flowing through layer p can also be written as

$$I_{\text{tot}} = A_{\|} \sum_{i} j_z^{pi} = gU \tag{204}$$

where the summation has to be carried out for all sites in layer p and the applied voltage U is given by

$$U = E_z^q d_{\perp} \tag{205}$$

with $A_{\|}$ and $d_{\perp}$ denoting the area of the two-dimensional unit cell and the interlayer spacing, respectively ($V_{at} = A_{\|} d_{\perp}$). Combining Eqs. (202), (204) and (205) results in an expression for the conductance,

$$g = \frac{1}{d_{\perp}^2} \sum_{i} \sum_{j} \sigma_{zz}^{pi, qj} \tag{206}$$

where the summations should, in principle, be carried out over all cells in layers p and q.

An alternative choice for the nonlocal conductivity tensor was given in Eq. (102), which is more practical in calculating the CPP conductance of a layered system than the nonlocal conductivity in the Kubo-Greenwood approach because, as shown by Baranger and Stone [9] for free electron leads, the second term appearing in Eq. (102) becomes identically zero when integrated over layers, $p \neq q$. This means also that the terms $\tilde{\sigma}_{\mu\mu}^{pi,qj}(\varepsilon^+, \varepsilon^+)$ and $\tilde{\sigma}_{\mu\mu}^{pi,qj}(\varepsilon^-, \varepsilon^-)$ should vanish after integration. It should be noted that very recently Mavropoulos et al. [20] rederived this result by assuming Bloch boundary conditions for the leads. According to these theoretical results, at zero temperature the diagonal elements of the nonlocal conductivity tensor between site i in layer p and site j in layer q can be written as

$$\sigma_{zz}^{pi,qj} = -\frac{1}{2}\tilde{\sigma}_{zz}^{pi,qj}(\varepsilon^+, \varepsilon^-) = \frac{\hbar}{2\pi}\int_{\Omega_{pi}} d^3 r_{pi} \int_{\Omega_{qj}} d^3 r'_{qj} Tr[J_z G^+(E_F; \mathbf{r}_{pi}, \mathbf{r}'_{qj}) J_z G^-(E_F; \mathbf{r}'_{qj}, \mathbf{r}_{pi})]$$

$$= \frac{\hbar}{2\pi} tr\left[\underline{J}_z^{pi}(\varepsilon^-, \varepsilon^+)\underline{\tau}_{\text{clus}}^{pi,qj}(\varepsilon^+)\underline{J}_z^{qj}(\varepsilon^+, \varepsilon^-)\underline{\tau}_{\text{clus}}^{qj,pi}(\varepsilon^-)\right] \tag{207}$$

such that the expression for the conductance reduces to

$$g = \frac{\hbar}{2\pi d_\perp^2}\sum_i \sum_j \int_{\Omega_{pi}} d^3 r_{pi} \int_{\Omega_{qj}} d^3 r'_{qj} Tr[J_z G^+(E_F; \mathbf{r}_{pi}, \mathbf{r}'_{qj}) J_z G^-(E_F; \mathbf{r}'_{qj}, \mathbf{r}_{pi})] \tag{208}$$

or, in terms of scattering path operators to

$$g = \frac{\hbar}{2\pi d_\perp^2}\lim_{\delta\to 0}\sum_i \sum_j tr\left[\underline{J}_z^{pi}(\varepsilon^-, \varepsilon^+)\,\underline{\tau}_{\text{clus}}^{pi,qj}(\varepsilon^+)\,\underline{J}_z^{qj}(\varepsilon^+, \varepsilon^-)\,\underline{\tau}_{\text{clus}}^{qj,pi}(\varepsilon^-)\right] \tag{209}$$

It has to be emphasized that because of the use of linear response theory and current conservation, the choice of layers p and q is arbitrary in Eqs. (208) and (209). If the layers p and q are asymptotically far away from each other, the above expressions naturally recover [20] the Landauer-Büttiker approach [3, 4], see section 2.2.

5. THE "LARGE CLUSTER" LIMIT

A real space version of Eq. (99) allows to study the interesting transition of electric transport properties from nanoscaled to macroscopic (mesoscopic) systems, simply by increasing the number of atomic sites included in the summation over sites. However, by doing so, such a procedure can also be used to document the numerical accuracy that can be achieved with a real space approach, since in the limit of two- or three-dimensional translational invariance corresponding theoretical results are available, obtained using appropriate lattice Fourier transformations. The following few sections serve exactly this purpose, namely to illustrate the convergence to semi-infinite and infinite systems.

5.1. Surface Layer of Ag(001)

The system studied is sketched in Fig. 2. The underlying parent lattice is an fcc structure corresponding to the experimental lattice spacing of fcc-Ag: $a_{3D} = 7.789$ a.u. and $a_{2D} = 5.508$ a.u.

The nonlocal conductivities in the surface layer were calculated according to Eqs. (183) and (184) with the real space scattering path operators being obtained by using 1830 $k_\parallel$ points in the two-dimensional irreducible wedge of the surface Brillouin zone. In Fig. 3, the xx and zz components of the nonlocal conductivity tensor $\sigma_{\mu\nu}^{0j}(x_j, y_j)$ are shown, where site 0 is fixed to the origin (0,0) of the surface layer, while the position of sites j is varied in the (001)-oriented surface plane. As can be seen, for the out of plane conductivity (zz), only scatterers are important which are not too far away from the origin, while in the in-plane case (xx) also scatterers at farther distances do add non-negligible contributions to the corresponding component of the conductivity. Moreover, it should be noted that the yy
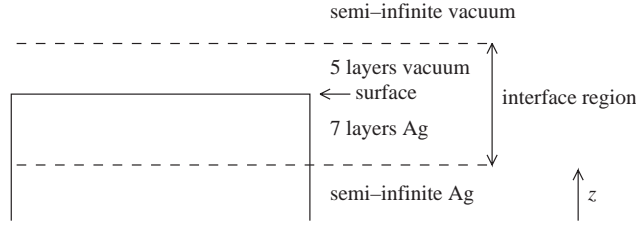
Figure 2. Geometrical setup of a semi-infinite Ag(001) system.

component is not shown because it is of similar form as the *xx* component: the diagram of $\sigma_{xx}^{0j}(x_j, y_j)$ simply has to be rotated by 90°.

The shape of the non-local conductivities suggests that by performing the summation in Eq. (194) only for sites within the chosen plane of atoms, it should converge according to Eq. (195). In order to show that, two different square-shaped planar clusters were investigated, see Fig. 4, both having C_{4v} symmetry which implies that $\rho_{\mu\mu}(r; \delta)$ has two independent components, namely

$$\rho_{xx} = \rho_{yy} \quad \text{and} \quad \rho_{zz} \tag{210}$$

The characteristic size (r) of the investigated clusters is given by the distance between the origin (0) and the farthermost atom from the origin, that is, can be viewed with respect to increasing sizes and fixed shape, namely in terms of $r_n = n \cdot a_{2D}$ for type 1 and $r_n = n\sqrt{2} \cdot a_{2D}$ for type 2, see Fig. 4. The number of atoms within a particular cluster is given by $N(n) = (2n^2 + 2n + 1)$ for type 1 and $N(n) = (4n^2 + 4n + 1)$ for type 2. Obviously, the clusters shown in Fig. 4 refer to $n = 3$. It has to be emphasized that this procedure is to show the validity of Eq. (195): as can be seen from Fig. 5, for both types of clusters a reliable convergence of the resistivity is achieved for $r > 15 \ a_{2D}$.
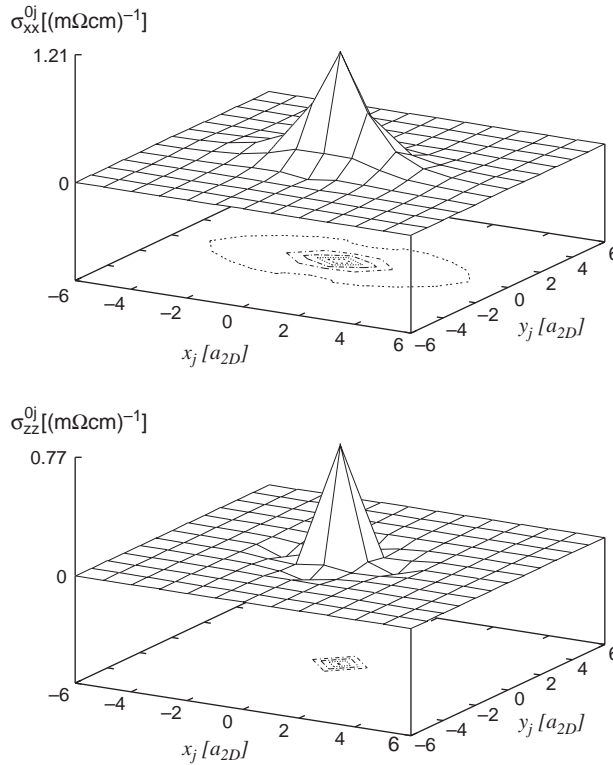
Figure 3. Nonlocal conductivity $\sigma_{xx}^{0j}(x_j, y_j)$ (top) and $\sigma_{zz}^{0j}(x_j, y_j)$ (bottom) corresponding to the surface layer of Ag. $\delta = 1$ mRy.

square type 1   square type 2
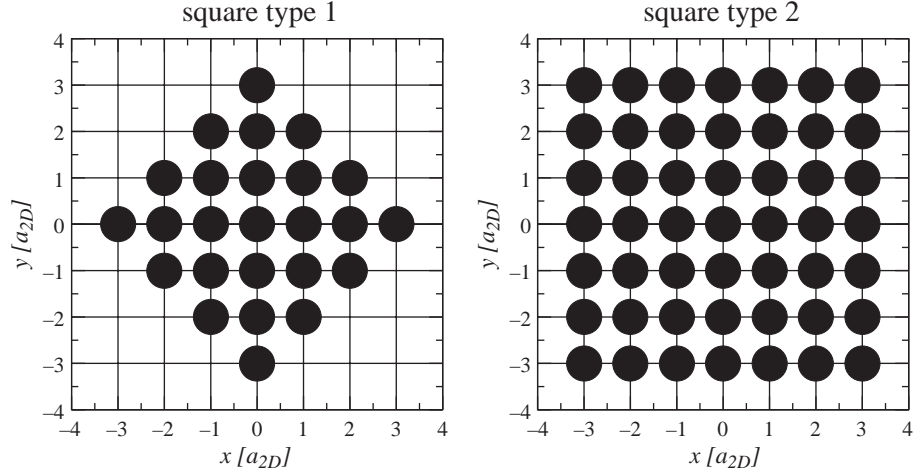
Figure 4. Square- and diamond-like shapes of a cluster in the surface plane of an fcc(001) substrate.

5.2. Bulk Resistivities

The studied systems are summarized in Fig. 6. The nonlocal conductivities were calculated according to Eq. (183) and the side limits in Eq. (184) for Ag and in Eqs. (190), (192) for CuPt alloys with the real space scattering path operators being obtained by using 630 $k_\parallel$ points in the two-dimensional irreducible wedge of the surface Brillouin zone. In the following, three-dimensional clusters are assumed; the real space summation of the non-local conductivity tensor was performed according to Eq. (194). In addition by increasing the size of the clusters the convergence of Eq. (198) was studied and the obtained results were
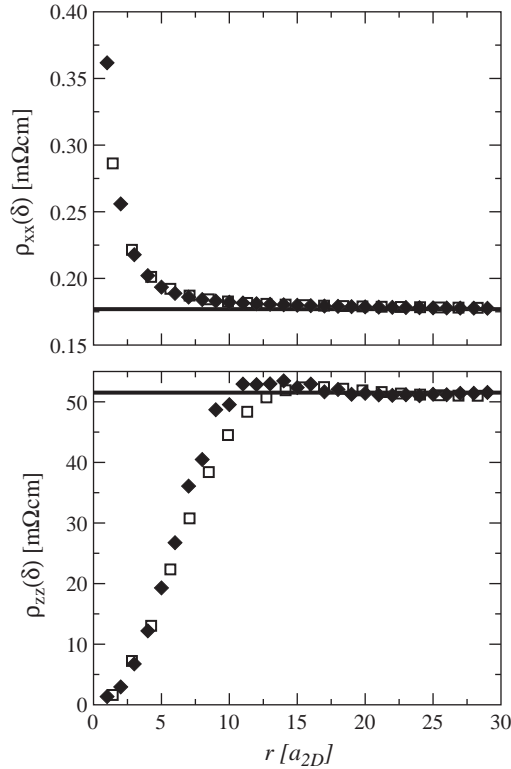
Figure 5. Convergence study in the surface layer of an Ag(001) semi-infinite system. The in-plane (xx) and perpendicular to the plane (zz) resistivity components for two different cluster shapes are shown *versus* the characteristic size of the cluster (r). The horizontal line refers to the layer-diagonal resistivity calculated by Eqs. (195)–(197). Diamonds correspond to type 1 in Fig. 4, squares to type 2, $\delta = 1$ mRy.
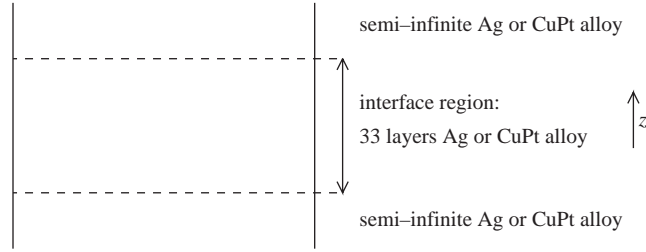
Figure 6. Geometrical setup of the Ag and CuPt bulk systems.

compared to known bulk resistivities, see Refs. [21, 22]. Clearly for large clusters the resistivity has to approach to the corresponding bulk value, namely to zero for pure metals and to the residual resistivity for (disordered) alloys. The clusters were chosen to be contained by a sphere of increasing radius; the origin of the spheres refers to the site denoted by 0 in Eq. (194). Table 1 shows the number of atoms (N) involved within a sphere with respect to n; the corresponding sphere radius r_n is defined by

$$r_n = \frac{n}{\sqrt{2}} \cdot a_{3D}$$

Assuming the following behavior of the elements of the resistivity tensor with respect to the size of the cluster (r),

$$\rho_{\mu\mu}(r; \delta) = \rho_0(\delta) + \frac{\rho_1(\delta)}{r} \tag{211}$$

ρ_0 and ρ_1 being constants, it is obvious that

$$r\rho_{\mu\mu}(r; \delta) = r\rho_0(\delta) + \rho_1(\delta) \tag{212}$$

which means that the residual resistivity, $\rho_0(\delta)$ can be obtained by a linear fit of $r\rho_{\mu\mu}(r; \delta)$ with respect to r. In the case of substitutional alloys, the slope ($\rho_0(\delta)$, $\delta \to 0$) corresponds then to the residual resistivity, while for a pure bulk it should be zero. It should be noted that Eq. (211) is more or less an empirical finding which was used also quite a bit also in the experimental recording of resistivities.

5.2.1. Ag Bulk

The fcc bulk Ag structure has the same lattice constants as mentioned in Section 5.1. In principle it is sufficient to evaluate only one component of the resistivity because the system and also the clusters have cubic symmetry, which means that by choosing the coordinate system properly, the resistivity tensor has only one independent element, that is, the diagonal components must be identical ($\rho_{xx} = \rho_{yy} = \rho_{zz}$). Deviations from this behavior can be used to estimate numerical errors inherent to the calculational scheme and the fitting procedure. The actual fitting, see Eq. (212), was performed for each calculated value of δ ($\delta = 1, 2, 3$ mRy) considering the last three points of $r\rho_{zz}(r; \delta)$, see top part of Fig. 7. These points have been chosen because they refer to the biggest clusters considered, see Table 1. In order to obtain the real physical residual resistivity an extrapolation to $\delta = 0$ is needed, see Eq. (193). This extrapolation for Ag bulk structure is illustrated in the top part of Fig. 8 and demonstrates that an absolute error of roughly 0.05 $\mu\Omega$cm was made in the applied fitting procedure.

Table 1. The number of sites (N) in clusters of spherical shape.

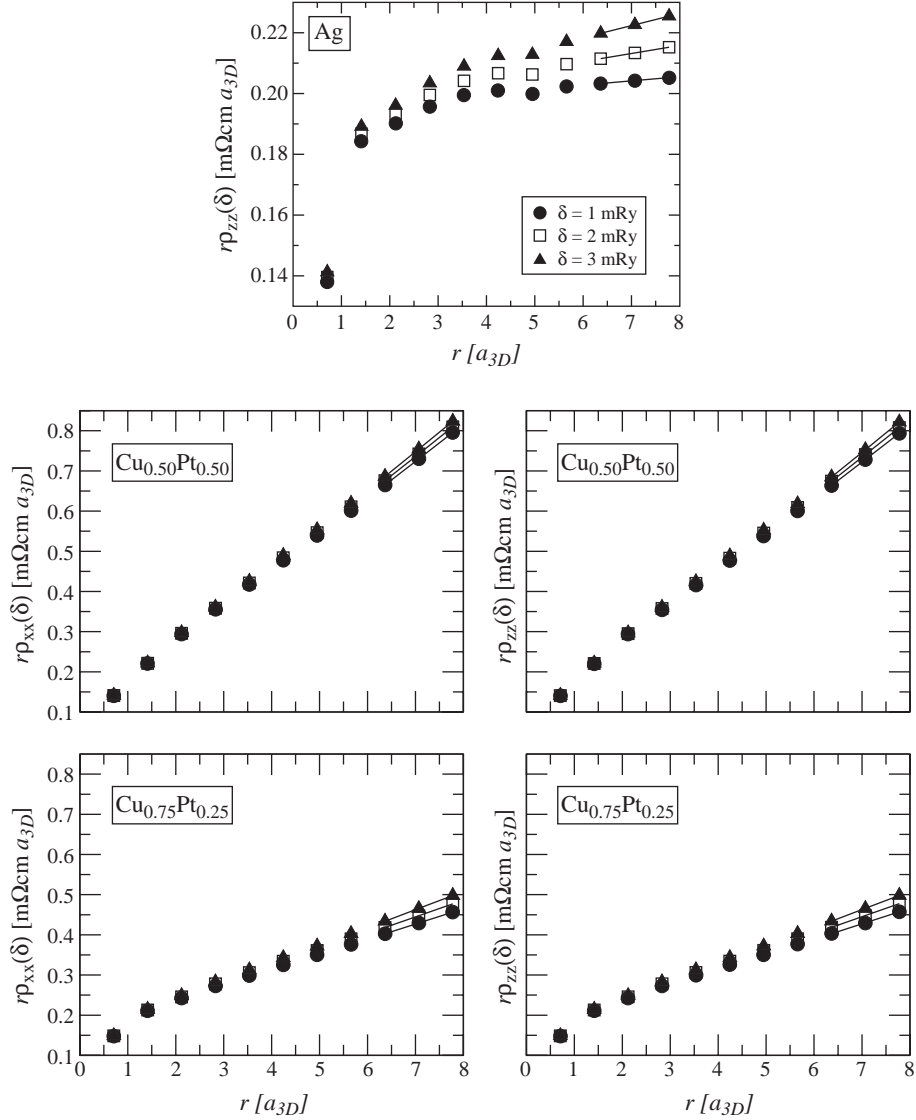|						Cluster						
n	0	1	2	3	4	5	6	7	8	9	10	11
$N(n)$	1	13	55	177	381	767	1289	2093	3055	4321	5979	7935

Figure 7. Convergence study in bulk systems. The characteristic size of the cluster (r) times the resistivity is shown *versus* the size of the cluster for three different imaginary parts (δ) of the Fermi energy in order to evaluate the slope (residual resistivity), see Eq. (212). The zz component of the resistivity is shown for fcc bulk Ag (top), and xx and zz components for fcc bulk CuPt alloys (bottom).

5.2.2. Cu_cPt_{1-c} Bulk

More interesting than pure bulk metals are disordered bulk alloys because the accuracy of the current approach can be directly compared with experimental data and results of previous calculations using three-dimensional periodic boundary conditions. For this reason, fcc $Cu_{0.50}Pt_{0.50}$ and $Cu_{0.75}Pt_{0.25}$ have been chosen with lattice constants $a_{3D}^{Cu_{0.50}Pt_{0.50}} = 7.140$ a.u. and $a_{3D}^{Cu_{0.75}Pt_{0.25}} = 6.995$ a.u. in order to test the reliability of the present approach. Again the fitting to a linear form to the last three points of $r\rho_{\mu\mu}(r)$ has been applied, see Eq. (212), as a function of δ, see the bottom part of Fig. 7. As can be seen, the extrapolation can easily be performed because in the region $0 < \delta < 3$ mRy the resistivity depends linearly on δ. In comparing the present results with previous calculations and available experimental data, see in particular Ref. [21], good quantitative agreement for both concentrations of CuPt is found: the results of Dulca et al. [22], for example, are 80.2 and 31.5 $\mu\Omega$cm for $Cu_{0.50}Pt_{0.50}$ and $Cu_{0.75}Pt_{0.25}$, respectively.

As already stated the numerical errors of the present approach can be judged best by determined by evaluating the difference between the in-plane and the perpendicular to the
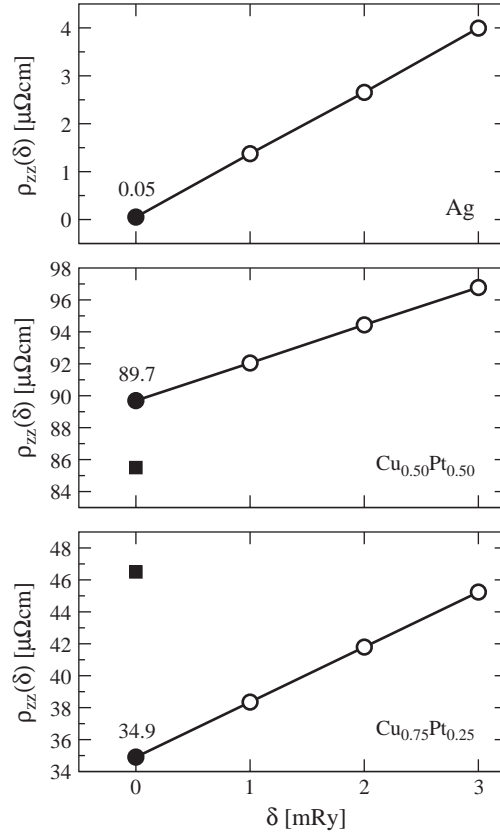
Figure 8. Extrapolation to $\delta = 0$ for the investigated bulk systems. Open circles are obtained from the fitting procedure in Eq. (212), while full circles refer to the extrapolated values. Squares denote experimental results measured at room temperature [21].

plane elements of the residual resistivity, since the residual resistivities, ρ_{xx} and ρ_{zz}, must be identical in cubic bulk systems. It can be seen from Fig. 9 that this difference is more or less independent of δ and is of order of a few tenth of a $\mu\Omega$cm.

6. MAGNETIC FINITE CHAINS IN THE SURFACE OF Ag(001)

In this section, single impurities and finite chains (length of 2–10 atoms) of Fe and Co embedded along the (110) direction (x) in the surface layer of Ag(001) are investigated, see also Fig. 2. In here, for matters of simplicity, a simple notation for the embedded chains is
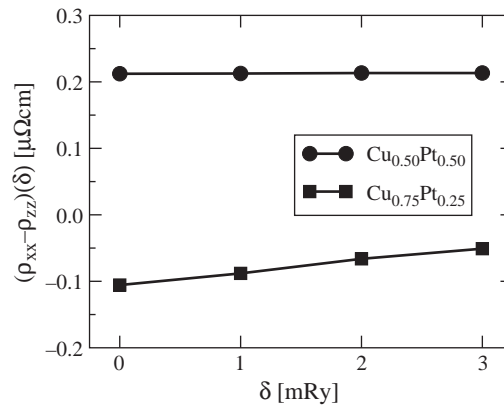
Figure 9. Difference between the residual resistivity for the in-plane (xx) and the perpendicular to the plane (zz) component *versus* the imaginary part (δ) of the Fermi energy for $Cu_{0.50}Pt_{0.50}$ and $Cu_{0.75}Pt_{0.25}$.
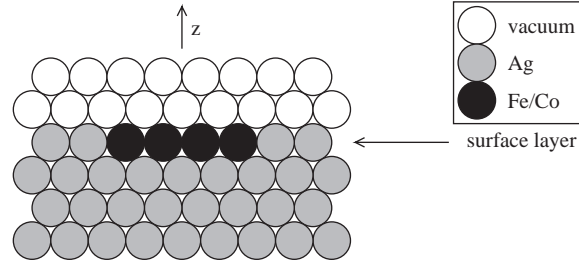
Figure 10. Chain of four atoms in the surface layer of Ag(001), $y = 0$ plane-section.

used, namely for example Co_4 for a Co chain of four atoms. For such a chain of four atoms the $y = 0$ plane-section of the system is shown in Fig. 10.

6.1. Nonlocal Conductivities

The influence of the chains to the in-plane transport in the surface layer was investigated by assuming a CIP geometry. The nonlocal conductivities were calculated according to Eq. (183), the scattering path operators of a specific cluster have been obtained in terms of the embedding equation, see Eq. (157). The real space host scattering path operators were
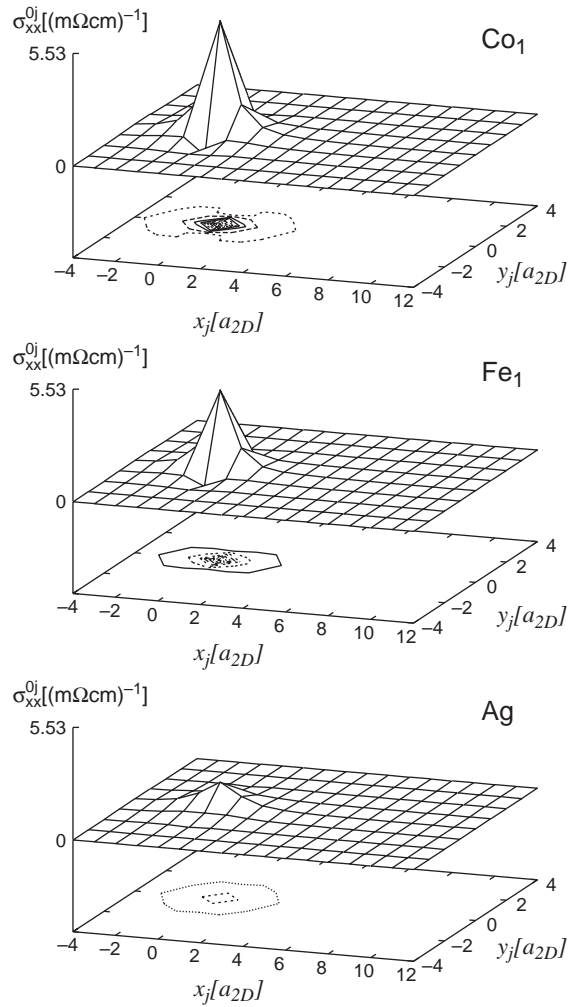
Figure 11. Nonlocal conductivities $\sigma_{xx}^{0j}(x_j, y_j)$ in the surface layer of Ag in presence of Co or Fe impurity at site 0 or without any impurities (pure Ag surface). $\delta = 1$ mRy, $\widehat{\mathbf{M}} = \hat{z}$.
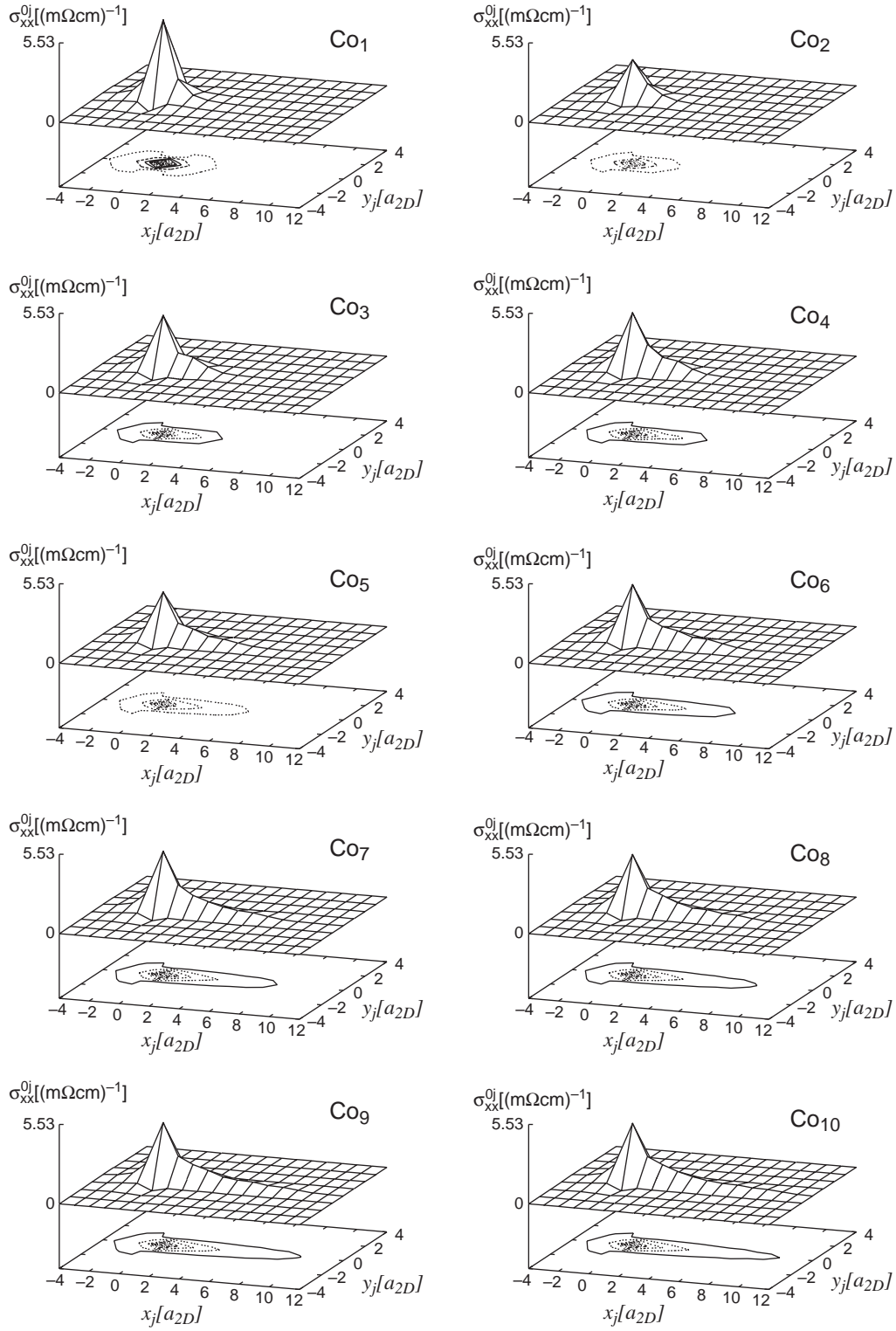
Figure 12. Nonlocal conductivities $\sigma_{xx}^{0j}(x_j, y_j)$ in the surface layer of Ag with Co atoms in a Co_n chain in positions $(0, 0), \ldots, (n-1, 0)$. $\delta = 1$ mRy, $\widehat{\mathbf{M}} = \hat{z}$.
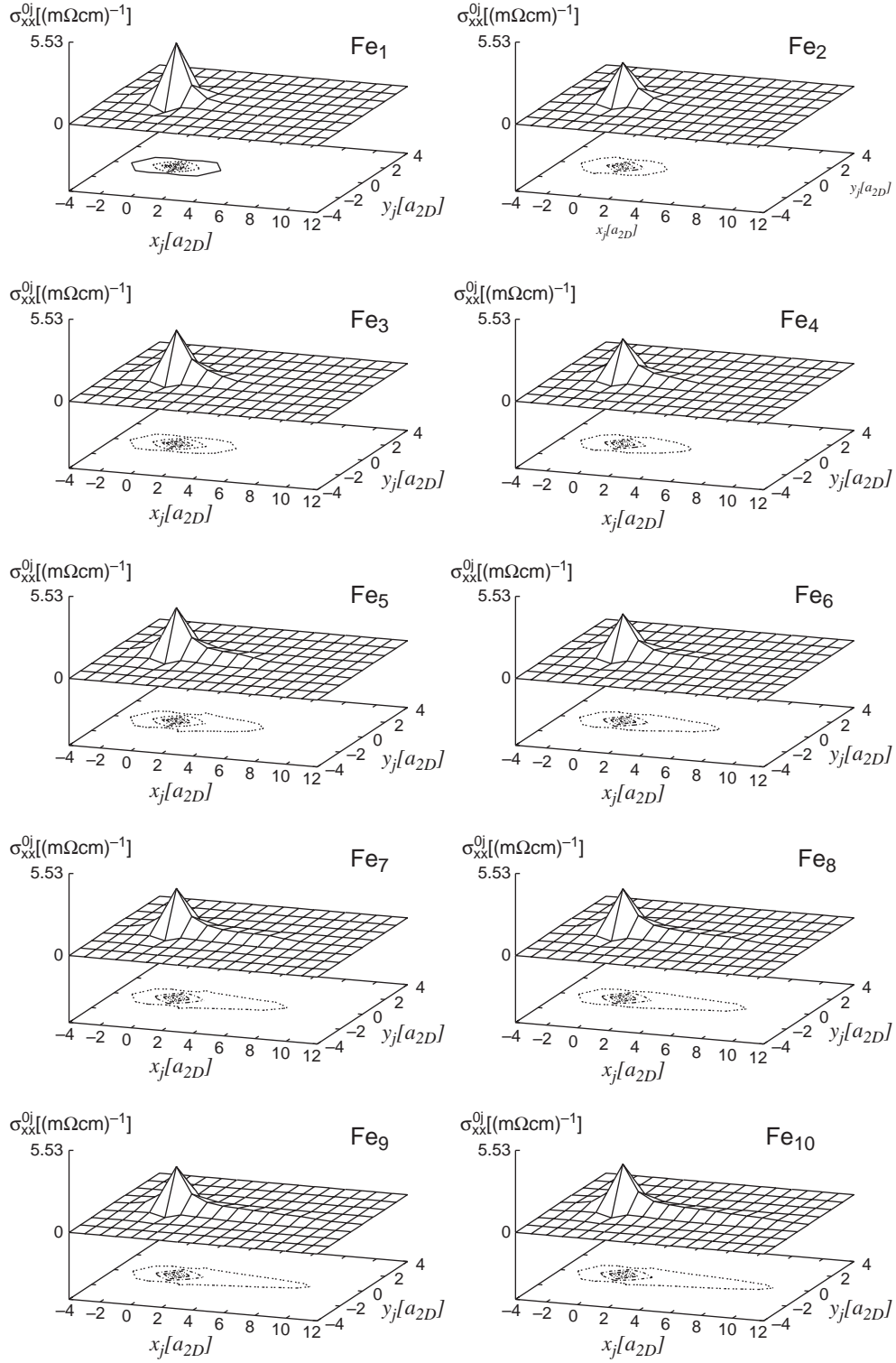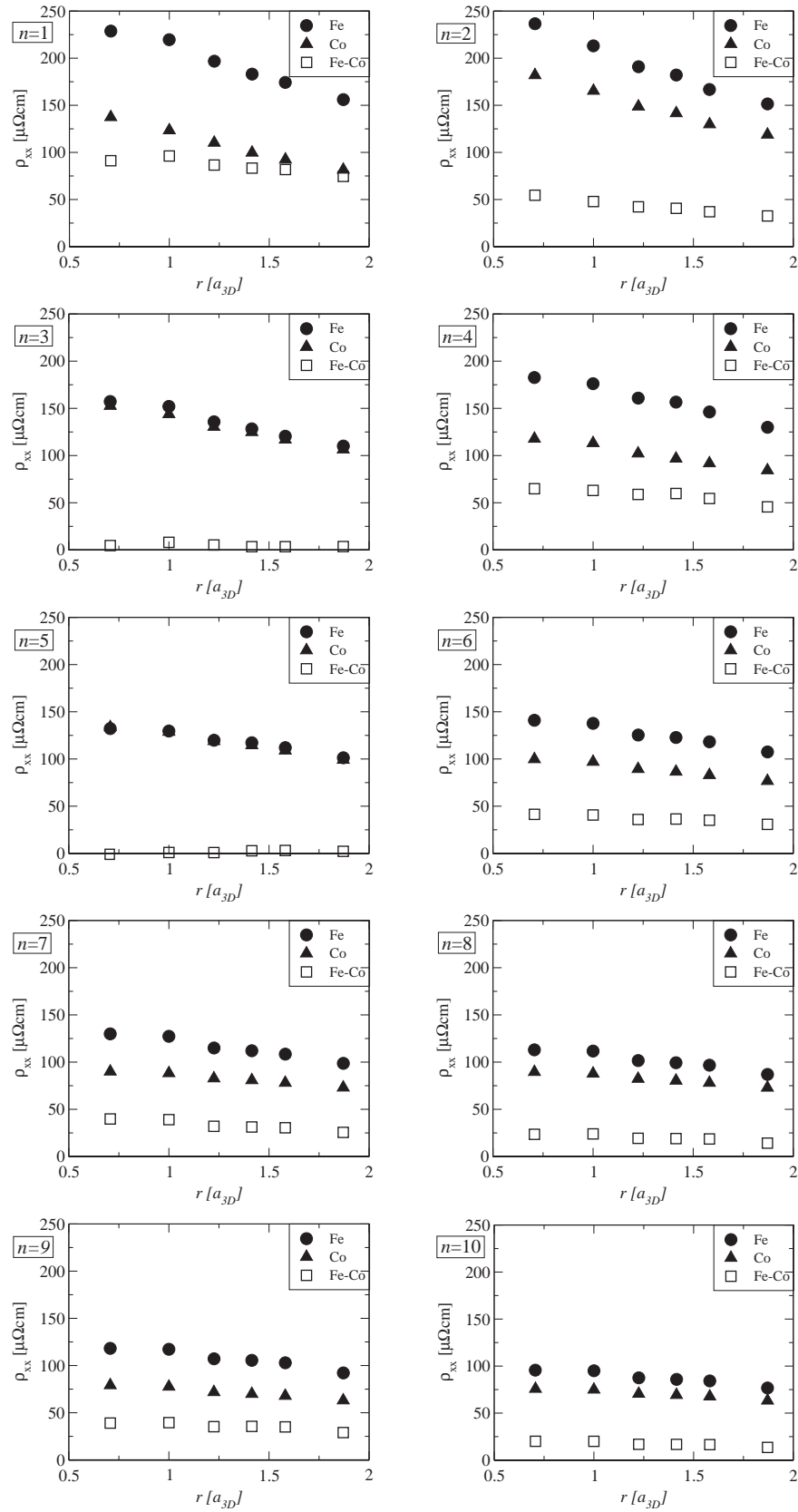
Figure 13. Nonlocal conductivities $\sigma_{xx}^{0j}(x_j, y_j)$ in the surface layer of Ag with Fe atoms in a Fe$_n$ chain in positions $(0, 0), \ldots, (n-1, 0)$. $\delta = 1$ mRy, $\widehat{\mathbf{M}} = \hat{z}$.

Figure 14. "Residual resistivities" of Fe (circles) and Co (triangles) chains. Open squares refer to $\rho_{xx}^{Fe}(r) - \rho_{xx}^{Co}(r)$. The length of the chains (n) is explicitly shown. $\delta = 0$ mRy (extrapolated), $\widehat{\mathbf{M}} = \hat{z}$.

calculated by using 210 $k_\parallel$ points in the two-dimensional irreducible wedge of the surface Brillouin zone.

Let 0 denote the origin in the surface plane ($x = 0$, $y = 0$), to which in the impurity case a single impurity is fixed. The xx-component of the nonlocal conductivity tensor between this site (0) and all the other atoms in the surface plane is shown in Fig. 11. As can be seen from this figure, the site-diagonal conductivity component of this site is larger for Co than for Fe, causing in turn of a higher resistivity of Fe chains after performing the summation in Eq. (213).

For chains the atom at the edge of a chain serves as origin, that is, it is located in the origin of the surface. The xx-component of the nonlocal conductivity tensor between this fixed site and all other atoms in the surface plane is shown in Fig. 12 for Co and in Fig. 13 for Fe. It can be seen that in the impurity case, the shape of the conductivity is symmetric to the $x = 0$ plane, whereas in the case of finite chains the tensor-elements along the $+x$ direction (where the chain lies) are much larger than in other directions, causing thus an asymmetry. This shape also implies that by summing up the nonlocal conductivity σ_{xx}^{0j} over sites j in a three-dimensional cluster around the chain, a significant contribution arises from the magnetic atoms. For a Co chain with length of six atoms, for example, the contribution from the magnetic atoms amounts to about 63%. Furthermore, it can also be seen that the magnitude of the site-diagonal conductivities decrease for atoms forming a chain as compared to the corresponding single impurity.

6.2. "Residual Resistivities"

In Section 4.4, a "residual resistivity" for finite clusters was defined as

$$\rho_{\mu\mu}^\alpha(r) = \left[\frac{1}{n} \sum_{i \in \text{chain}} \sum_{j=1}^{N(r)} \sigma_{\mu\mu}^{ij} \right]^{-1} \tag{213}$$

where n denotes the number of atoms in the chain of type α (Fe or Co), and $N(r)$ is the number of atoms involved in the cluster (chain + environmental atoms up to the furthermost distance of r). It should be noted that for evaluating Eq. (213) three-dimensional clusters have to be used. Obviously, the convergence properties of $\rho_{\mu\mu}^\alpha(r)$ with respect to r can be investigated by increasing size of the cluster. This is shown in Fig. 14. As can be seen in this figure $\rho_{xx}^\alpha(r)$ decreases for all chain lengths (n) monotonously and can in principle be extrapolated to large values of $N(r)$, see Eq. (212), while the difference, $\rho_{xx}^{Fe}(r) - \rho_{xx}^{Co}(r)$ remains finite and varies only slowly with respect to the cluster size. Furthermore, chains with length of three or five atoms differ distinctly from the rest, namely there is almost no difference whether Fe or Co atoms form the chain, i.e., the difference, $\rho_{xx}^{Fe}(r) - \rho_{xx}^{Co}(r)$ nearly vanishes for all cluster size considered.

The "residual resistivity" of finite clusters defined in Eq. (213) is a practical tool to study the influence of in-plane transport properties with respect to the orientation of magnetization ($\widehat{\mathbf{M}}$). The calculated results of the xx-component of the resistivity are listed in Table 2.

Table 2. "Residual resistivities" *versus* orientation of magnetization ($\widehat{\mathbf{M}}$), $\rho_{xx}(r = a_{3D})[\mu\Omega\text{cm}]$ in Co and Fe chains, $\delta = 0$ mRy (extrapolated).

Length	Co			Fe		
	$\hat{x}$	$\hat{y}$	$\hat{z}$	$\hat{x}$	$\hat{y}$	$\hat{z}$
1	120.1	126.9	123.5	198.3	225.3	219.6
2	162.6	162.2	165.4	200.5	213.1	213.2
3	151.4	140.1	143.9	142.0	153.8	152.0
4	109.0	113.7	113.2	166.7	176.4	176.2
5	122.6	126.6	128.8	122.2	130.1	129.7
6	94.9	100.1	97.0	132.3	138.6	137.6
7	85.6	89.7	88.3	119.5	125.9	127.3
8	86.1	89.4	87.8	108.0	111.9	111.7
9	74.0	78.6	77.6	110.2	114.7	117.1
10	73.4	77.2	74.9	91.3	93.4	94.9

As can be seen, $\widehat{\mathbf{M}} = \hat{x}$, i.e., $\widehat{\mathbf{M}}$ parallel to the orientation of the chains provides the smallest resistivity for all Fe chains and for the most Co chains. There are two exceptions where this does not apply, namely Co_2 and Co_3. For these chains the smallest resistivity is obtained for $\widehat{\mathbf{M}} = \hat{y}$. This behavior is quite surprising in view of the resistivities for the other chains. In most cases the direction of magnetization $\widehat{\mathbf{M}} = \hat{y}$ seems to yield the highest resistivity, however, the orientation of magnetization perpendicular to the chain ($\hat{y}$ and $\hat{z}$) results in minor differences in the resistivity. Moreover, in the impurity case, $\rho_{xx}^{Fe}(\hat{y})$ is by 13.6% larger than $\rho_{xx}^{Fe}(\hat{x})$, whereas $\rho_{xx}^{Co}(\hat{y})$ is only by 5.7% larger than $\rho_{xx}^{Co}(\hat{x})$, which means a higher sensitivity with respect to the orientation of the magnetization for the Fe impurity.

7. NANOCONTACTS

Nanocontacts made of gold are presumably the most studied atomic-sized conductors in the literature. A dominant peak very close to the conductance quantum, $1\ G_0 = 2e^2/h$, has been reported for gold in the conductance histogram [23, 24] and attributed to the highly transmitting sp channel across a linear monoatomic chain connecting the two electrodes. In this section, gold contacts are investigated in different geometries as well as the influence of transition metal impurities on the conductance is studied within the real-space approach described in Sections 4.1 and 4.5.

The host system for the embedding is shown in Fig. 15. It should be noted that all of the considered sites (Au, vacuum and impurities) refer to the positions of an underlying ideal fcc structure of gold with a lattice constant of $a_{3D} = 7.681$ a.u.

A schematic view of a typical contact is displayed in Fig. 16 with $N_V = 5$ vacuum layers considered in the host system, see Fig. 15. As follows from the above, atomic sites refer to layers for which the following notation is used: C denotes the *central layer*, $C - 1$ and $C + 1$ the layers below and above, and so forth. The contact consists of a central layer that contains 1 Au atom (the rest is built up from empty spheres); layers $C - 1$ and $C + 1$, see Fig. 17a, contain 4 Au atoms, layers $C - 2$ and $C + 2$ 9 Au atoms, and, though not shown, all other layers, namely $C - n$ and $C + n$ ($n \geq 3$), are completely filled with Au atoms, that is, denote full layers. The nonlocal conductivities were calculated according to Eq. (207), the scattering path operators of a specific cluster were obtained by the embedding equation, Eq. (157). The real space host SPOs were calculated by taking 210 $k_\parallel$ points in the two-dimensional irreducible wedge of the surface Brillouin zone.

7.1. Numerical Tests for Different Gold Contacts

As mentioned in Section 4.1, a finite Fermi level broadening, δ, has to be used for the nonlocal conductivity, thus, also for conductance calculations. As an example, for the point contact depicted in Fig. 17a, the dependence of the conductance on δ is investigated. The summation in Eq. (209) was carried out up to convergence for the first two (symmetric) full layers ($p = C - 3$, $q = C + 3$). As can be seen from Fig. 18, the calculated conductances depend strongly but nearly linear on δ. A straight line fitted for $\delta \geq 1.5$ mRy intersects the vertical axis at 2.38 G_0. Assuringly enough, a calculation with $\delta = 1$ μRy resulted in $g = 2.40 G_0$. Although the nearly linear dependence of the conductance with respect to δ
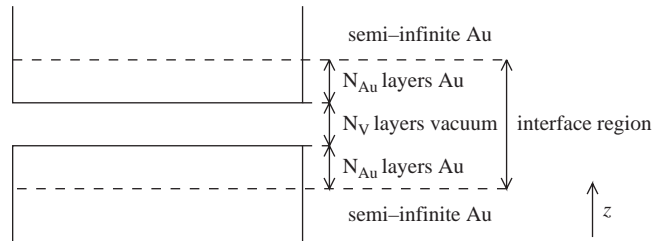

Figure 15. Geometrical setup of Au(001) host system. A nanojunction between the two semi-infinite systems is modeled by embedding Au atoms into the vacuum region, see, for example, Figs. 16 and 17. The host characterized by N_{Au} and N_V sites that can be different for different contacts.
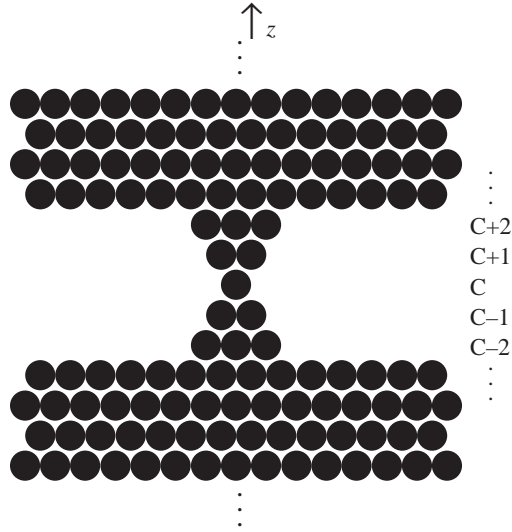
Figure 16. Schematic side view of a point contact between two semi-infinite leads embedded into the vacuum region (number of vacuum layers $N_V = 5$). The layers are labeled by C, $C \pm 1$, and so forth.

enables an easy extrapolation to $\delta = 0$, in the following all reported conductances refer to $\delta = 1 \, \mu$Ry.

For the same type of contact (Fig. 17a), the convergence of the summation in Eq. (209) over layers p and q was investigated, choosing different symmetric pairs of full layers. The convergence with respect to the number of atoms in the layers is shown in Fig. 19. Convergence for about 20 atoms can be obtained for the first two full layers ($p = C - 3$, $q = C + 3$), whereas the number of sites needed to get convergent sums gradually increases if one includes layers farther away from the contact atom. This kind of convergence property is qualitatively understandable, as the current flows from the contact within a cone of some opening angle that cuts out sheets of increasing area from the corresponding layers. As all the calculations were performed with $\delta = 1 \, \mu$Ry, current conservation has to be expected. Consequently, the calculated conductance ought to be independent with respect to the layers chosen for the summation in Eq. (209). As can be seen from Fig. 19 this is satisfied within a relative error of less than 10%. It should be noted, however, that for the pairs of layers, $p = C - n$, $q = C + n$, $n \geq 6$ convergence was not achieved within this accuracy: by taking
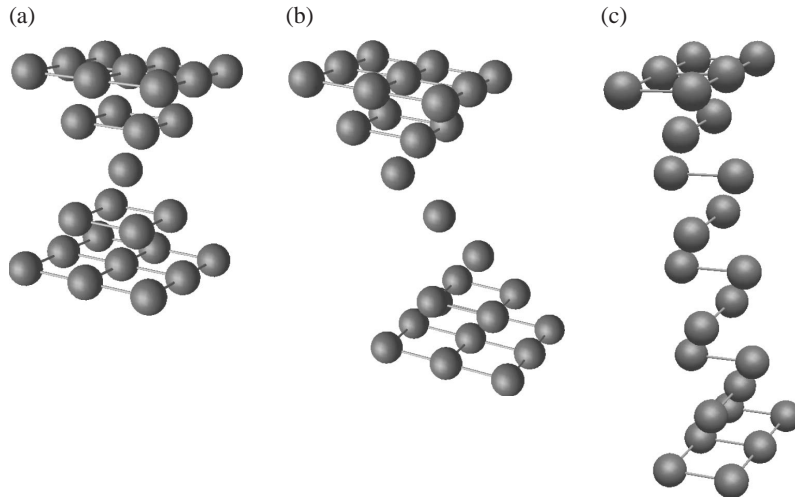

Figure 17. Perspective view of some of the studied contacts between two fcc(001) semi-infinite leads. Only the partially filled layers are shown. (a) point contact (number of Au layers taken into account: $N_{Au}=5$, number of vacuum layers between the leads: $N_V = 5$. (b) Slanted linear finite chain ($N_{Au} = 7$, $N_V = 7$). (c) 2×2 finite chain ($N_{Au} = 6$, $N_V = 9$).
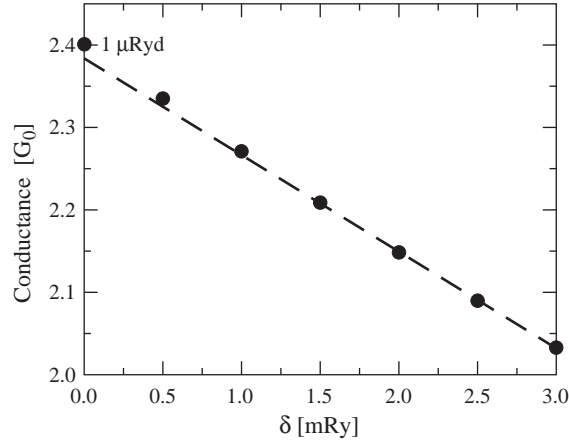
Figure 18. Calculated conductance as a function of the Fermi level broadening δ for the Au contact shown in Fig. 17a. The dashed straight line is a linear fit to the values for $\delta = 1.5, 2.0, 2.5,$ and 3.0 mRy.

more sites in the summations even a better coincidence of the calculated conductance values for different pairs of layers can be expected. Figure 19 also implies that an application of the Landauer-Büttiker approach to calculate the conductance of nanocontacts is numerically more tedious than the present one, since, in principle, two layers situated infinitely far from each other have to be taken in order to represent the leads.

Although only one Au atom is placed in the center of the point contact considered above, see Fig. 17a, the calculated conductance is more than twice as large as the conductance unit. This is easy to understand since the planes $C - 1$ and $C + 1$, each containing four Au atoms, are relatively close to each other and, therefore, tunneling contributes quite a lot to the conductance through the contact. In order to obtain a conductance around 1 G_0, detected in the experiments, a linear chain has to be considered. The existence of such linear chains is obvious from the long plateau of the corresponding conductance trace with respect to the piezo voltage in the break-junction experiments. Because at present the computer code for the real space Kubo equation is restricted to geometrical structures confined to three-dimensional translational invariant simple bulk parent lattices, as the simplest model of such a contact a slanted linear chain was considered as shown in Fig. 17b. In there, the middle layer (C) and the adjacent layers ($C \pm 1$) contain only one Au atom, layers $C \pm 2$ and $C \pm 3$ four and nine Au atoms, respectively, whereas layers $C \pm 4$ refer to the first two full layers. The sum in Eq. (209) was carried out for two pairs of layers, namely for $p = C - 4, q = C + 4$ (full layers) and for $p = C - 2, q = C + 2$ (not full layers). The convergence with respect to the number of atoms in the chosen layers can be seen from Fig. 20. The respective converged
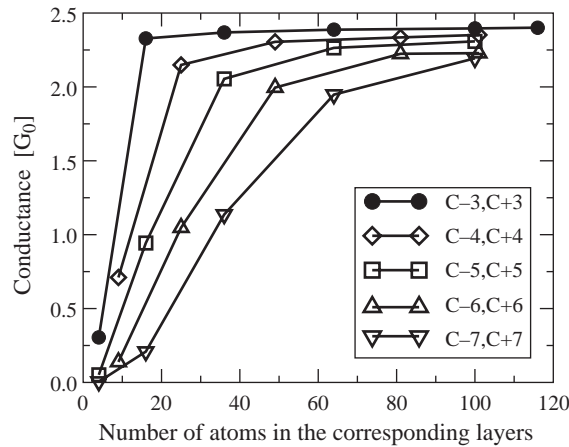

Figure 19. Conductance *versus* the number of sites included in the sum in Eq. (209) for the contact in Fig. 17a. The different curves show conductances as calculated between different pairs of layers. For a definition of the layer numbering see Fig. 16.
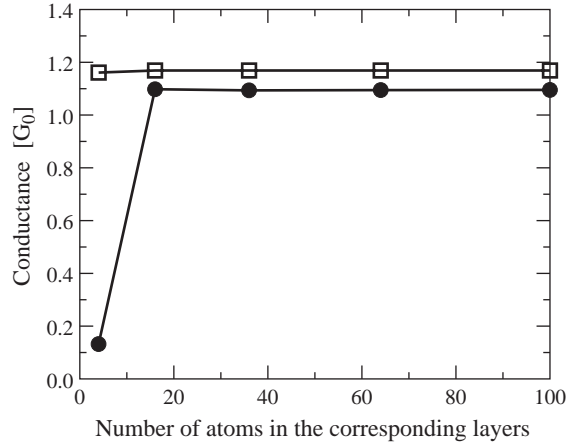
Figure 20. Conductance *versus* the number of sites included in the sum in Eq. (209) for the slanted linear chain shown in Fig. 17b. Full circles are the results of summing in layers $p = C - 4$ and $q = C + 4$ (first full layers), and squares refer to a summation in layers $p = C - 2$ and $q = C + 2$ (layers containing four Au atoms).

values are 1.10 G_0 and 1.17 G_0. In the case of $p = C - 2$, $q = C + 2$ the contribution from the vacuum sites is nearly zero: considering only four Au atoms in the summation already gave a value for the conductance very close to the converged one. The small difference between the two calculated values, 0.07 G_0, most likely has to be attributed to the use of the atomic sphere approximation (ASA). Nevertheless, as expected, the calculated conductance is very close to the ideal value of 1 G_0.

Another interesting structure is the 2×2 chain described in Ref. [25], namely the structure depicted in Fig. 17c. The conductance for this structure was calculated by including to the summation 100 atoms from each of the first two full layers. As result a conductance of 2.58 G_0 was obtained. Papanikolaou et al. [25] got a conductance of 3 G_0 for an infinite Cu wire to be associated with three conducting channels within the Landauer approach. For an infinite wire the transmission probability is unity for all states, therefore, the conductance is just the number of bands crossing the Fermi level. For the present case of a finite chain, the transmission probability is less than unity for all the conducting states. This qualitatively explains the reduced conductance with respect to an infinite wire.

Finally, the dependence of the conductance on the thickness of the nanocontacts was studied. All the investigated structures have C_{4v} symmetry and the central layer of the systems is a plane of reflection symmetry. The set-up of the structures is summarized in Table 3. Contact 0 refers to a broken contact which is embedded into a host with $N_{Au} = 7$ and $N_V = 7$ layers, see Fig. 15, while the others have different thicknesses from 1 up to 9 Au atoms in the central layer, and are embedded into a host characterized by $N_{Au} = 5$ and $N_V = 5$, see Fig. 15.

In Fig. 21, the calculated conductances are displayed as performed by including nearly 100 atoms from each of the first two full layers: $p = C - 4$, $q = C + 4$ for the broken contact and $p = C - 3$, $q = C + 3$ for all the other cases, see Table 3. It can be seen that the conductance

Table 3. Set-up of various nanocontacts.

Layer position	Contact				
	0	1	4	5	9
$C \pm 4$	Full	Full	Full	Full	Full
$C \pm 3$	9	Full	Full	Full	Full
$C \pm 2$	4	9	16	21	25
$C \pm 1$	1	4	9	12	16
C	0	1	4	5	9

Shown is the number of Au atoms in the layers as labeled by C, C $\pm$ 1, etc., see Fig. 16. Contact 1 refers to Fig. 17a.
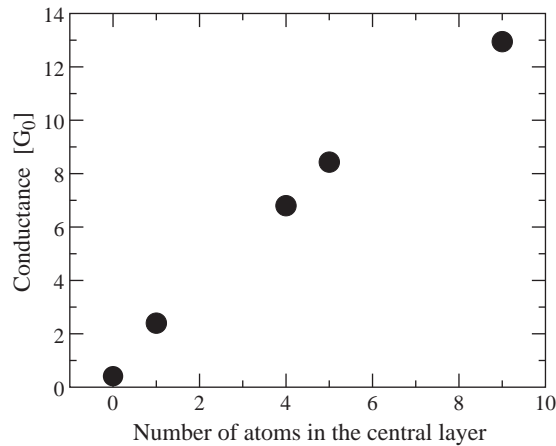
Figure 21. Conductance *versus* the number of Au atoms in the central layer for the Au contacts described in Table 3.

is almost proportional to the number of Au atoms in the central layer. This finding can qualitatively be compared with the result of model calculations for the conductance of a three-dimensional electron gas through a connective neck as a function of its area in the limit of $\vartheta_0 = 90°$ for the opening angle [26]. In the case of the broken contact, the nonzero conductance can again be attributed to tunneling of electrons.

7.2. Gold Contact with an Impurity

In recent break junction experiments [27], remarkable changes of the conductance histograms of nanocontacts formed from AuPd alloys have been observed when varying the Pd concentration. Studying the effect of impurities placed into the nanocontact are, in that context, at least relevant for dilute alloys. The interesting question is whether the presence of impurities can be observed in the measured conductance. For that reason we investigated transition metal impurities such as Pd, Fe, and Co placed at various positions of the point contact as shown in Fig. 17a. For the notation of the impurity positions, see Fig. 22.

The calculated spin and orbital moments of the magnetic impurities are listed in Table 4. They were calculated with assuming the direction of magnetization to be parallel to the z axis ($\widehat{\mathbf{M}} = \hat{z}$), that is, normal to the planes. Additional calculations of the magnetic anisotropy energy confirmed this choice. As usual for magnetic impurities with reduced coordination number [28], both for Fe and Co remarkably high spin moments, and in all positions of a Co impurity large orbital moments were obtained. In particular, the magnitude of the orbital moments is very sensitive to the position of the impurity. This is most obvious in the case of Fe, where at positions B and C the orbital moment is relatively small, but at position A a surprisingly high value of 0.47 μ_B was obtained.

The summation over 116 atoms from each of the first two full layers ($p = C - 3$, $q = C + 3$) in Eq. (209) has been carried out in order to evaluate the conductance. The calculated values are summarized in Table 5.
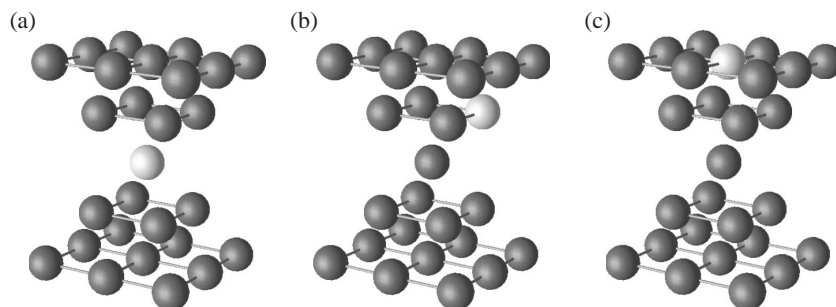

Figure 22. Impurity positions (light gray spheres) in a Au point contact, see Fig. 17a.

Position	$S_z[\mu_B]$		$L_z[\mu_B]$	
	Fe	Co	Fe	Co
A	3.36	2.01	0.47	0.38
B	3.46	2.17	0.04	0.61
C	3.42	2.14	0.07	0.22

A Pd impurity (independent of position) reduces only little the conductance as compared to a pure Au point contact. This qualitatively can be understood from the local density of states (LDOS) of the Pd impurity as calculated for an imaginary part of the energy of $\delta = 1$ mRy, the real space scattering path operators by using 1830 $k_\parallel$ points in the 2D IBZ. It should be noted that the LDOS at site i (n_i) is defined as follows

$$n_i(\varepsilon) = \mp \frac{1}{\pi} \int_{\Omega_i} d^3 r \, Im[G^{\pm}(\varepsilon, \mathbf{r}, \mathbf{r})] \tag{214}$$

where Ω_i denoted the volume of the ith unit cell. In Fig. 23, the corresponding LDOS at positions A and C is plotted. Clearly, the change of the coordination number (8 at position A and 12 at position C), that is, different hybridization between the Pd and Au d bands, results into different widths for the Pd d-like LDOS. In both cases, however, the Pd d states are completely filled and no remarkable change in the LDOS at Fermi level (conducting states) happens.

The case of magnetic impurities seems to be more interesting. As can be inferred from Table 5, impurities at position B change only very little the conductance. Being placed at position A, however, Fe and Co atoms increase the conductance by 11% and 24%, whereas at position C they decrease the conductance by 19% and 27%, respectively. In Ref. [25] it was found that single Fe, Co (and also Ni) defects in a 2×2 infinite Cu wire decreased the conductance. By analyzing the DOS, it was concluded that the observed reduction of the conductance is due to a depletion of the s-like states in the minority band. The above situation is very similar to the case of an Fe or Co impurity in position C of the point contact considered, even the calculated drop of the conductance ($\sim -20\%$ for Fe and $\sim -28\%$ for Co) agrees quantitatively well with our present result. Our result, namely, that Fe and Co impurities at position A increase the conductance, however, *cannot* be related to the results of Ref. [25]. In order to understand this feature, one carefully has to investigate the LDOS calculated for the point contact.

In Fig. 24, the minority d-like LDOS of the Fe and Co impurities in positions A and C are plotted as resolved according to the canonical orbitals $d_{x^2-y^2}$, d_{xy}, d_{xz}, d_{xy} and $d_{3z^2-r^2}$. It has to be pointed out strongly that this kind of partial decomposition, usually referred to as the (ℓ, m, s) representation of the LDOS, is not unique within a relativistic formalism, since due to the spin-orbit interaction different spin- and orbital components are mixed. However, due to the large spin-splitting of Fe and Co the mixing of the majority and minority spin-states can be neglected.

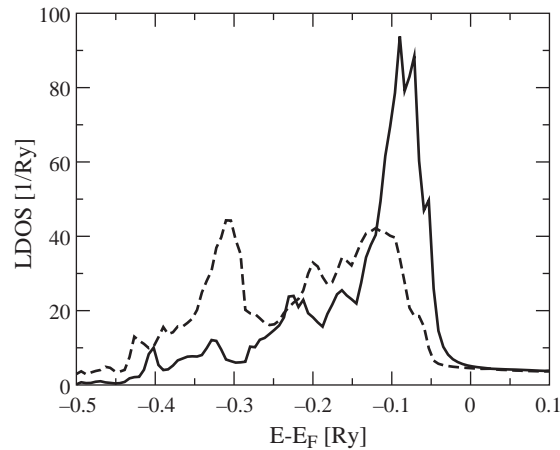| Impurity position	Conductance $[G_0]$		
	Pd	Fe	Co
A	2.22	2.67	2.97
B	2.24	2.40	2.26
C	2.36	1.95	1.75
Pure Au		2.40	

Figure 23. Local density of states of a Pd impurity in position A (solid line) and in position C (dashed line) of a Au point contact, see Fig. 22.

As can be seen from Fig. 24, the LDOS of an impurity in position A is much narrower than in position C. This is an obvious consequence of the difference in the coordination numbers (8 for position A and 12 for positions C). Thus an impurity in position A hybridizes less with the neighboring Au atoms and, as implied by the LDOS, the corresponding d states are fairly localized. Also to be seen is a spin-orbit induced splitting of about 8 mRy ($\sim$0.1 eV) in the very narrow $d_{x^2-y^2}$-d_{xy} states of the impurities in position A. The difference of the band filling for the two kind of impurities shows up in a clear downward shift of the LDOS of Co with respect to that of Fe.

In Fig. 25, a comparison between a nonrelativistic and a relativistic calculation is displayed: the splitting in the $d_{x^2-y^2}$ and d_{xy} states vanishes by turning off the spin-orbit coupling.
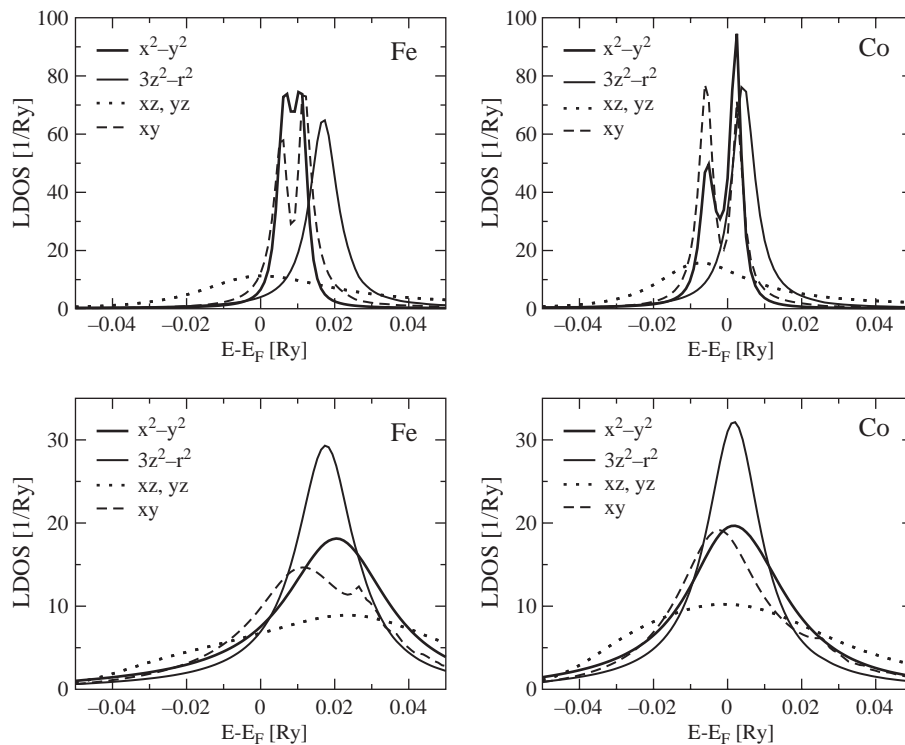

Figure 24. Minority-spin orbital-resolved d-like local density of states of Fe and Co impurities in position A (upper panels) and in position C (lower panels) of a Au point contact, see Fig. 22.
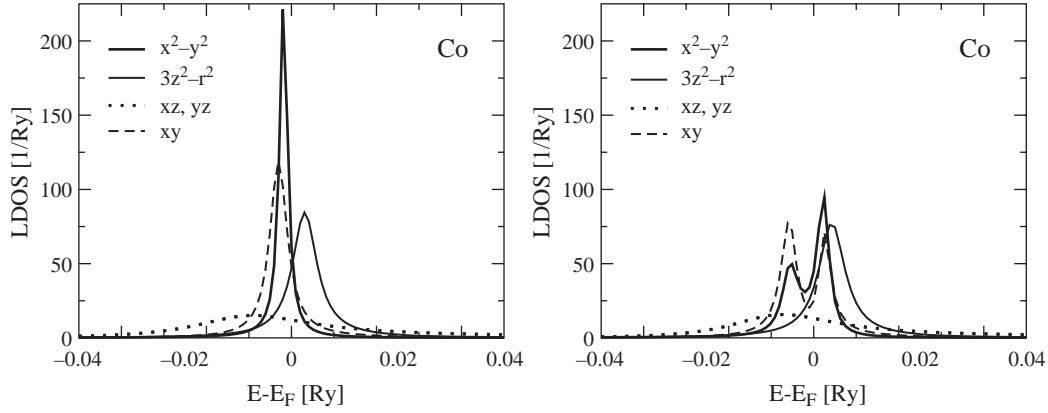
Figure 25. Minority-spin orbital-resolved d-like local density of states of a Co impurity in position A, see Fig. 22. On the left nonrelativistic, on the right relativistic calculation is displayed.

In order to explain the change in the conductance through the point contact caused by impurities in positions A and C, the s-like DOS at the center site, that is, at the narrowest section of the contact, is plotted in the top half of Fig. 26. As a comparison, the corresponding very flat s-like DOS is shown for a pure Au contact. For contacts with impurities this s-like DOS shows a very interesting shape, which can indeed be correlated with the corresponding $d_{3z^2-r^2}$-like DOS at the impurity site, see bottom half of Fig. 26. As clearly can be seen, the center positions and the widths of the $d_{3z^2-r^2}$-like DOS peaks and those of the respective (anti-)resonant s-like DOS shapes coincide well with each other. This kind of behavior in the DOS resembles the case studied by Fano for a continuum band and a discrete energy level in the presence of configuration interaction (hybridization) [29]. Apparently, by
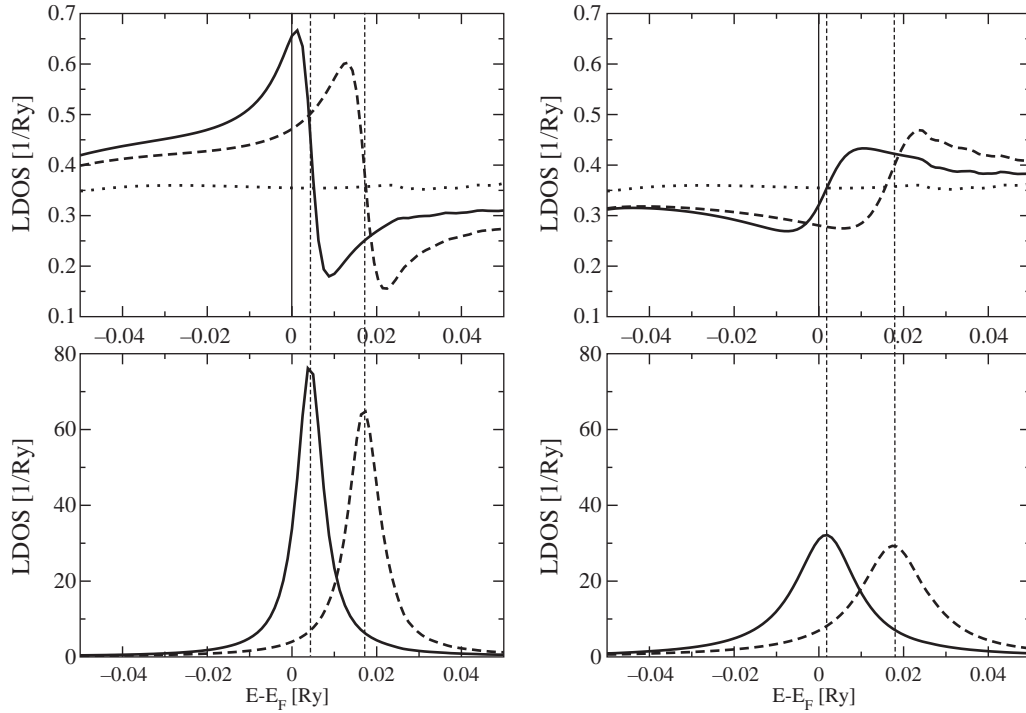

Figure 26. Top left: minority-spin s-like local density of states at the center site of a Au point contact with an impurity at position A, see Fig. 22 (solid line: Co, dashed line: Fe). Top right: the same as before, but with an impuritiy at position C. As a comparison, in both figures the corresponding LDOS for the pure Au contact is plotted by dotted lines. The solid vertical lines highlight the position of the Fermi energy. Bottom: minority-spin $d_{3z^2-r^2}$ local density of states of the impurities (solid line: Co, dashed line: Fe) at positions A (left) and C (right). Vertical dashed lines mark the center positions of the $d_{3z^2-r^2}$-LDOS peaks.

keeping this analogy, in the point contact the s-like states play the role of a continuum and the $d_{3z^2-r^2}$-like state of the impurity acts as the discrete energy level. Because these this two kinds of states share the same cylindrical symmetry, interactions between them can occur due to backscattering effects. It should be noted that similar resonant line-shapes in the STM I-V characteristics have been observed for Kondo impurities at surfaces [30, 31] and explained theoretically in Ref. [32].

Inspecting Fig. 26, the enhanced s-like DOS at the Fermi level at the center of the point contact provides a nice interpretation for the enhancement of the conductance when an Fe and Co impurity is placed at position A. As the peak position of the $d_{3z^2-r^2}$-like states of Fe is shifted upwards by more than 0.01 Ry with respect to that of Co, the corresponding resonance of the s-like states is also shifted and the s-like DOS at the Fermi level is decreased. This is also in agreement with the calculated conductances. In the case of impurities at position C, that is, in a position by $a_{3D} = 7.681$ a.u. away from the center of the contact, the resonant line-shape of the s-like states is reversed in sign, therefore, one observes a decreased s-like DOS at the Fermi level, explaining in this case the decreased conductance, see Table 5. As, however, the s-like DOS for the case of a Co impurity is larger than for an Fe impurity, this simple picture cannot account correctly for the opposite relationship obtained for the corresponding conductances.

8. CONCLUSIONS

In the current paper, methods and approaches were introduced and discussed in order to describe the electric properties of "real space" nanostructures, that is, of systems with a finite number of atoms properly embedded in (metallic) substrates. It is indeed important to note that whenever structures nanoscaled in two dimensions (finite supported clusters) are considered, the influence of the substrate has to be taken into account. Furthermore, because in particular finite magnetic nanostructures (very small islands) are of technological interest, a relativistic approach has to be applied in order to describe adequately the orientation of the magnetization in these structures on all levels (electronic structure, electric transport). The last example shown, namely atom-sized contacts, refers to a topic that will be of increasing importance in many applications, in particular, since the conducting properties of such contacts can be modulated quite a bit by placing impurities in the very vicinity of the actual contact atoms.

ACKNOWLEDGMENTS

REFERENCES

1. P. Weinberger, *Physics Reports* 377, 281 (2003).
2. N. F. Mott, *Adv. Phys.* 13, 325 (1964).
3. R. Landauer, *IBM J. Res. Dev.* 1, 223 (1957); *Z. Phys. B* 21, 247 (1975); *Z. Phys. B* 68, 217 (1987); *IBM J. Res. Dev.* 32, 306 (1988); *J. Phys. Condens. Matter* 1, 8099 (1989).
4. M. Büttiker, *Phys. Rev. Lett.* 57, 1761 (1986); IBM *J. Res. Dev.* 32, 317 (1988).
5. R. Kubo, M. Toda, and N. Hashitsume, "Statistical Physics II: Non-equilibrium Statistical Mechanics." Springer, Berlin, 1985; R. Kubo, *J. Phys. Soc. Jpn.* 12, 570 (1957).
6. J. M. Luttinger, in "Mathematical Methods in Solid State and Superfluid Theory" (Oliver and Boyd, Eds.), pp. 157. Edinburgh, 1962.
7. D. A. Greenwood, *Proc. Phys. Soc. London* 71, 585 (1958).
8. W. H. Butler, *Phys. Rev. B* 31, 3260 (1985).
9. H. U. Baranger and A. D. Stone, *Phys. Rev. B* 40, 8169 (1989).

10. J. Zabloudil, R. Hammerling, L. Szunyogh, and P. Weinberger, "Electron Scattering in Solid Matter, a Theoretical and Computational Treatise," 1st Edn., Springer, 2004.
11. M. E. Rose, "Relativistic Electron Theory." Wiley, New York, 1961.
12. A. Messiah, "Quantum Mechanics." North Holland, Amsterdam, 1969.
13. S. L. Altmann and P. Herzig, "Point Group Theory Tables." Oxford, 1994.
14. G. A. Korn and T. M. Korn "Mathematical Handbook for Scientists and Engineers." McGraw-Hill, New York, 1961.
15. B. L. Györffy and M. J. Stott, in "Band Structure Spectroscopy of Metals and Alloys" (D. J. Fabian and L. M. Watson, Eds.), Academic Press, London, 1973.
16. L. Szunyogh, B. Újfalussy, P. Weinberger, and J. Kollár, *Phys. Rev. B* 49, 2721 (1994).
17. R. Zeller, P. H. Dederichs, B. Újfalussy, L. Szunyogh, and P. Weinberger, *Phys. Rev. B* 52, 8807 (1995).
18. L. Szunyogh, B. Újfalussy, and P. Weinberger, *Phys. Rev. B* 51, 9552 (1995).
19. P. Weinberger, P. M. Levy, J. Banhart, L. Szunyogh, and B. Újfalussy, *J. Phys.: Condens. Matter* 8, 7677 (1996).
20. P. Mavropoulos, N. Papanikolaou, and P. H. Dederichs, *Phys. Rev. B* 69, 125104 (2004).
21. J. Banhart, H. Ebert, P. Weinberger, and J. Voitländer, *Phys. Rev. B* 50, 2104 (1994).
22. L. Dulca, J. Banhart, and G. Czycholl, *Phys. Rev. B* 61, 16502 (2000).
23. J. M. Krans, I. K. Yanson, Th. C. M. Govaert, R. Hesper, and J. M. van Ruitenbeek, *Phys. Rev. B* 48, 14721 (1993).
24. M. Brandbyge, J. Schiøtz, M. R. Sørensen, P. Stoltze, K. W. Jacobsen, J. K. Nørskov, L. Olesen, E. Laegsgaard, I. Stensgaard, and F. Besenbacher, *Phys. Rev. B* 52, 8499 (1995).
25. N. Papanikolaou, J. Opitz, P. Zahn, and I. Mertig, *Phys. Rev. B* 66, 165441 (2002).
26. J. A. Torres, J. I. Pascual, and J. J. Sáenz, *Phys. Rev. B* 49, 16581 (1994).
27. A. Enomoto, S. Kurokawa, and A. Sakai, *Phys. Rev. B* 65, 125410 (2002).
28. B. Lazarovits, L. Szunyogh, and P. Weinberger, *Phys. Rev. B* 65, 104441 (2002).
29. U. Fano, *Phys. Rev.* 124, 1866 (1961).
30. V. Madhavan, W. Chen, T. Jamneala, M. F. Crommie, and N. S. Wingreen, *Science* 280, 567 (1998).
31. H. C. Manoharan, C. P. Lutz, and D. M. Eigler, *Nature* 403, 512 (2000).
32. O. Újsághy, J. Kroha, L. Szunyogh, and A. Zawadowski, *Phys. Rev. Lett.* 85, 2557 (2000); O. Újsághy, G. Zaránd, and A. Zawadowski, *Solid State Commun.* 117, 167 (2001).